# Enhanced seismic base isolation using inertial amplifiers

Sudip Chowdhury[a], Arnab Banerjee[b,*], Sondipon Adhikari[c]

[a] *PhD Scholar, Civil Engineering Department, IIT Delhi, India. Email: sudip.chowdhury@civil.iitd.ac.in*
[b] *Assistant Professor, Civil Engineering Department, IIT Delhi, India. Email: abanerjee@iitd.ac.in*
[c] *Professor, Aerospace Engineering Department, Swansea University, UK. Email: s.adhikari@swansea.ac.uk*

**Abstract**

Harnessing the concept of inertial amplification, an inertial amplifier coupled base isolator (IABI) is proposed in this paper. The seismic performance, in terms of story drift, base shear reduction, of this proposed inertial amplifier coupled base isolator has been compared with that of the classical base isolator (CBI) and inerter-based isolation system (Inerter-BI). A thorough analytical study, implementing rationals of random vibration for harmonic and Gaussian white noise is conducted to identify the performance of the inertial amplifier coupled base isolator (IABI) in the frequency domain. Further, a numerical study is conducted to determine the story drift, base shear response in time-domain for the inertial amplifier based base-isolated structure and classical base-isolated structure for twenty-two real earthquake ground motions. The results elucidate the histogram of base shear and story drift reduction percentage shifts towards higher values for inertial amplifier coupled isolator compared to CBI and Inerter-BI. From both analytical and numerical study, it is observed that the seismic performance and response reduction capacity of proposed IABI is significantly 89.38% and 72% superior to the classical base isolator and inerter-based isolation system, respectively. This finding evidenced towards the supremacy of the inertial amplifier base isolator over the classical base isolator and inerter coupled base isolator in terms of seismic vibration control.

*Keywords:* Inertial amplification; Inertial amplifier coupled base isolator; Stochastic analysis; Classical base isolator, Inerter-based isolation system.

## 1. Introduction

The base isolation systems are installed between the structure and foundation to control the seismic responses of the structure. Touaillon's [1] isolation system can be considered as the historical origin of the base isolation system where the base isolator was modelled as double concave spherical sliding bearing isolation system in 1870. The classical base isolation system can be mathematically modelled as a viscously damped two degree of freedom system and its generalized solution is served as the baseline for the designing of the multilayered elastomeric bearings for seismic isolation [2, 3]. Decoupling of the structures from the earthquake ground motions is the essence of the seismic base-isolation towards the minimization of inter-story drift and floor accelerations[4]. An appropriate design of the base isolation device absorbs and/ or dissipate a significant part of the seismic energy [5, 6]. The base isolation devices were exhaustively studied, and widely acclaimed since 1990 [4]. Simplified but useful comprehension can be developed from the analytical solution of a linear classical base isolator [7] consists of two degrees of freedom system with springs, masses and viscous dampers. Additionally, non-viscous [8] or viscoelastic [9] damping in the context of vibration reduction were also studied and found that [10] a optimally designed viscoelastic tuned-mass damper can out perform a classical viscous tuned-mass damper. Although not investigated in this work, non-viscous or viscoelasticaly damped systems may have the potential for enhanced isolation. The nonlinear isolators can be perceived by altering the viscous dampers of the linear system with hysteresis damping [11–13]. Lead rubber bearing [14], New Zealand bearing [15], Friction-Pendulum system [16], Resilient Friction Base Isolator [17] and Pure-Friction system [18] are some examples of the nonlinear base isolation devices which results in the hysteresis damping. Among the nonlinear systems friction pendulum system (FPS) is provided a larger isolation period which makes

*Corresponding author

the base of the isolated structure more flexible and its high re-centring capacity decouples the mass of the main structure from the ground during earthquakes [19–23].

On the other hand, an inerter is applied in the traditional vibration control devices to enhance its energy dissipation capacity by massive effective mass amplification through rotational mass with motion transformers [24, 25] inside the system. The inerter was first introduced by Smith [26, 27] from the force to the current analogy for mitigation of vibration responses of the structures. Since then, these inerters have widely been implemented in mechanical systems as vibration control devices, especially for automobiles [28–33]. Recently, Kuhnert et al. [34] critically reviewed the advantages and disadvantages of the inerter-based vibration isolation systems. Most of the previous inerter based isolation devices are made by flywheel-gear inerter [35, 36]. Inerters were often used in conjunction with other vibration control devices to enhance its performance [37, 38]. For example, Qian et al. [35] enhance the seismic performance of a base-isolated structure with a tuned inerter damper [39]. The seismic performance of the base-isolated structures have been enriched by incorporating the inerter-based systems [40, 41]. In this context, the inerter has induced inside the traditional Friction Pendulum system (FPS) system [42] and it is observed that the vibration reduction capacity of traditional FPS has increased [43, 44]. Not only for the building frames, the inerter-based isolation systems can also be mitigated the vibrations of the water storage tanks [40, 45, 46] during any seismic events. These inerter-based isolation systems for vibration control of multi-storied building [47] can be modelled with helical springs and Čakmak et al. [48] studied the vibration fatigue analysis of inerter-based isolation system with helical spring. To optimize the governing parameters of the inerter based base-isolator, $h_2$ [36] and $h_\infty$ [49] optimization schemes are widely acclaimed.

Apart form the inerter, massive mass amplification can also be obtained by inertial amplifiers and a large wide bandgap will occur at low frequencies [50–53]. This inertial amplifier based isolation system is entirely different [36] from the widely acclaimed flywheel-gear inerter [35, 41]. The characteristics of widen band gaps at low frequencies allows these amplifiers to surpass the vibration of low frequency based periodic lattice structures [52, 54–56], acoustic insulation of walls[57, 58], beams [59–62] etc. However, the application of these inertial amplifier in massive civil engineering structure like building [63] and bridges is not extremely studied. Recently, Cheng et al. [64] enhanced a tuned mass damper (TMD) with the help of inertial amplifier mechanism (IAM) and the results showed that the seismic performance of IAM-TMD is superior to the traditional TMD [65–68]. However, an inertial amplifier coupled base isolator is not presented in the existing state of the art.

An inertial amplifier coupled base isolator is introduced in this paper. The massive effective mass amplification occurs due to the geometry of the inertial amplifier which enhanced the vibration reduction capacity of the proposed IABI. The frequency domain and stochastic responses have been evaluated analytically while the time-domain responses are produced numerically. The sensitivity analysis considering system parameters of proposed IABI have been conducted to investigate the effectiveness of system parameters on structural responses. The dynamic responses of the uncontrolled and controlled structures are compared to evaluate the vibration reduction capacity of the each isolators. In the present study, the vibration mitigation capacity of the inertial amplifier coupled base isolator is evaluated compared to that of the classical base isolator and inerter-based isolation system [40].

## 2. Structural model and Equations of motion

The schematic diagrams of structures isolated by classical base isolator (CBI), inerter-based isolation system (Inerter-BI), and inertial amplifier coupled base isolator (IABI) are presented in Figure 1 (a), (b) and (c). It is considered that the isolated structures are subjected to ground motions $\ddot{u}_g$.

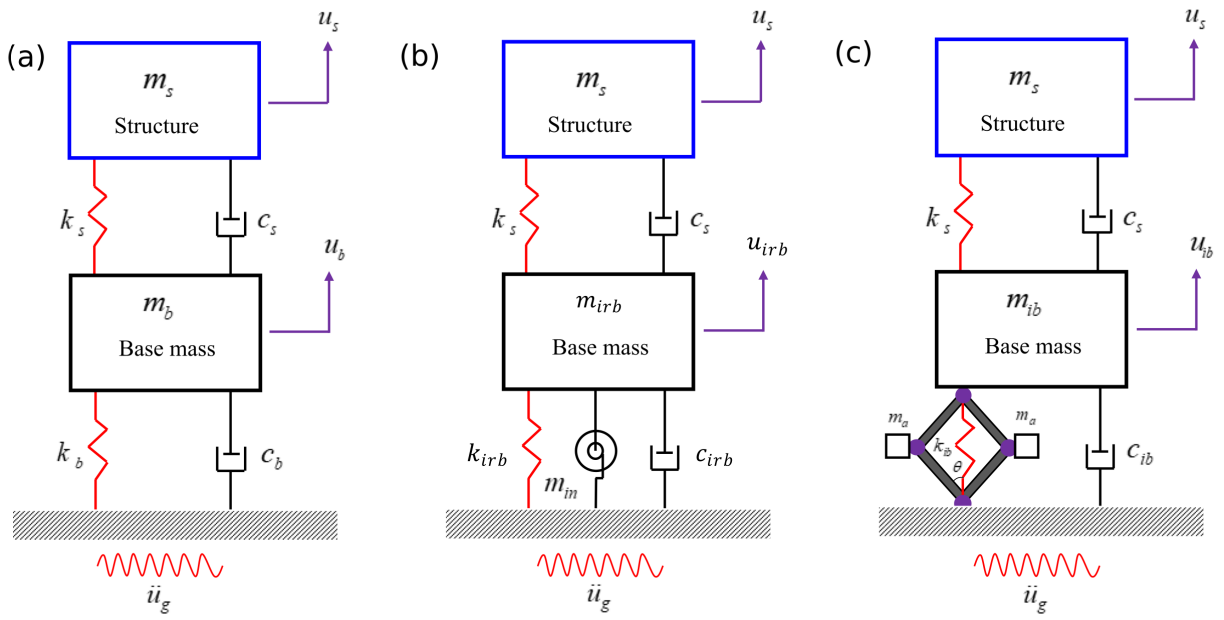


**Figure** 1: Schematic diagrams of dynamic systems isolated by (a) classical base isolator, (b) inerter-based isolation system, (c) inertial amplifier coupled base isolator.

In Figure 1 (a), $m_b$, $c_b$, $k_b$ refer the base mass, damping, and stiffness of the CBI. $u_s$ and $u_b$ refer the displacement of structure and CBI. In Figure 1 (b), $m_{irb}$, $c_{irb}$, $k_{irb}$ refer the base mass, damping, and stiffness of the Inerter-BI, and $m_{in}$ indicates the mass of the inerter. $u_s$ and $u_{irb}$ refer the displacement of structure and Inerter-BI. In Figure 1 (c), $m_{ib}$, $c_{ib}$, $k_{ib}$ refer the base mass, damping, and stiffness of the IABI. $\theta$ indicates the inertial angle between the y- axis and the rigid links when the isolated structure is in undeformed state. $u_s$ and $u_{ib}$ refer the of structure and IABI. $m_s$, $c_s$, and $k_s$ refer the mass, damping, and stiffness of the main dynamic systems for all isolated systems presented in Figure 1.

### *2.1. Structures isolated by classical base isolators*

The responses of the structure isolated by inertial amplifier coupled base isolator are compared with the responses of structure isolated by classical base isolator. The structural parameters are contained similar and the damping and total mass ratios of both isolators are retained similar.

$$\begin{aligned} m_b\ddot{y}_b + c_b\dot{y}_b + k_b y_b - k_s y_s - c_s\dot{y}_s &= -m_b\ddot{u}_g \\ m_s\ddot{y}_s + c_s\dot{y}_s + k_s y_s &= -m_s(\ddot{u}_g + \ddot{y}_b) \end{aligned} \tag{1}$$

where, $y_b = u_b - u_g$ and $y_s = u_s - u_b$. $(\dot{\bullet})$ defines the derivative with respect to time. The isolated structure is subjected to a harmonic base motion. The relative displacement of the structure and the base isolator in Eq. (1) can be considered as $y_s = Y_s e^{\mathrm{i}\omega t}$ and $y_b = Y_b e^{\mathrm{i}\omega t}$. The function of ground accelerations are considered as $u_g = U_g e^{\mathrm{i}\omega t}$. In the displacement notations, $Y_s$, $Y_b$, and $U_g$ are the displacement amplitudes of the structure, base isolator, and the ground motion. After substituting the values in Eq. (1), the equation of motion can be expressed as:

$$\begin{aligned} q^2 m_b Y_b + q c_b Y_b + k_b Y_b - k_s Y_s - q c_s Y_s &= -q^2 m_b U_g \\ q^2 m_s Y_s + q^2 m_s Y_b + q c_s Y_s + k_s Y_s &= -q^2 m_s U_g \end{aligned} \tag{2}$$

where $q = \mathrm{i}\omega$. The transfer function can be evaluated as:

$$\begin{bmatrix} A_{11} & A_{12} \\ A_{21} & A_{22} \end{bmatrix} \begin{Bmatrix} Y_s \\ Y_b \end{Bmatrix} = -q^2 \begin{bmatrix} 1 \\ \mu_b \end{bmatrix} U_g \tag{3}$$

$$A_{11} = 2\,\zeta_s q\omega_s + q^2 + {\omega_s}^2; A_{12} = q^2; A_{21} = -2\,\zeta_s q\omega_s - {\omega_s}^2; A_{22} = \mu_b q^2 + 2\,\zeta_b q\omega_b\,(\mu_b + 1) + \omega_b^2\,(\mu_b + 1) \tag{4}$$

Isolator parameters are considered as: isolator mass ratio to the structure $\mu_b = \frac{m_b}{m_s}$, damping ratio of the base isolator $\zeta_b$ which can be calculated from $\zeta_b = \frac{c_b}{2\omega_b M}$, $M = m_s + m_b$, $\epsilon_b = (\frac{\omega_b}{\omega_s})^2$. The displacement responses of the structure and base isolator are obtained as:

$$H_s(q) = \frac{Y_s}{U_g} = \frac{-q^2\left(\mu_b+1\right)\left(2\,\zeta_b q\omega_b + \omega_b^2\right)}{\Delta_b} \tag{5}$$

$$H_b(q) = \frac{Y_b}{U_g} = \frac{-q^2\left(\ 2\,q\zeta_s\mu_b\omega_s + \mu_b q^2 + 2\,\zeta_s q\omega_s + \mu_b {\omega_s}^2 + {\omega_s}^2\ \right)}{\Delta_b} \tag{6}$$

$$\begin{aligned}\Delta_b = {} & 2\,\zeta_s\omega_s\left(\mu_b+1\right)q^3 + \left({\omega_s}^2+\omega_b^2\right)\left(\mu_b+1\right)q^2 + 2\,\zeta_s\omega_s\omega_b^2\left(\mu_b+1\right)q \\ & + \omega_b^2{\omega_s}^2\left(\mu_b+1\right) + 2\,q\zeta_b\left(2\,\zeta_s q\omega_s + q^2 + {\omega_s}^2\right)\left(\mu_b+1\right)\omega_b + q^4\mu_b\end{aligned} \tag{7}$$

The shear force can be obtained as:

$$H_{sf}(q) = \frac{q\zeta_s Y_s + \omega_s^2 Y_s}{U_g} = \frac{\left(\ -q^2\left(\mu_b+1\right)\left(2\,\zeta_b q\omega_b + \omega_b^2\right)\left(q\zeta_s + {\omega_s}^2\right)\ \right)}{\Delta_b} \tag{8}$$

The transfer matrix in Eq. (3) can be represented as fully non-dimensional manner and presented as:

$$\begin{bmatrix} \tilde{A}_{11} & \tilde{A}_{12} \\ \tilde{A}_{21} & \tilde{A}_{22} \end{bmatrix} \begin{Bmatrix} Y_s \\ Y_b \end{Bmatrix} = \eta^2 \begin{bmatrix} 1 \\ \mu_b \end{bmatrix} U_g \tag{9}$$

$$\tilde{A}_{11} = -\eta^2 + 2\,i\zeta_s\eta + 1; \tilde{A}_{12} = -\eta^2; \tilde{A}_{21} = -2\mathrm{i}\zeta_s\eta - 1; \tilde{A}_{22} = -\mu_b\eta^2 + 2\mathrm{i}\zeta_b\eta\sqrt{\epsilon_b}\left(\mu_b+1\right) + \epsilon_b\left(\mu_b+1\right) \tag{10}$$

The non-dimensional displacement responses are evaluated as:

$$H_s(\eta) = \frac{Y_s}{U_g} = \frac{-\eta^2\left(2\mathrm{i}\zeta_b\eta\sqrt{\epsilon_b} + \epsilon_b\right)\left(\mu_b+1\right)}{\Delta_{b1}} \tag{11}$$

$$H_b(\eta) = \frac{Y_b}{U_g} = \frac{-\eta^2\left(\ -\mu_b\eta^2 + \mu_b + 1 + \mathrm{i}\left(2\,\eta\,\zeta_s\mu_b + 2\,\zeta_s\eta\right)\ \right)}{\Delta_{b1}} \tag{12}$$

$$\begin{aligned}\Delta_{b1} = {} & 2\,\left(\mu_b+1\right)\zeta_b\left(\eta^2\mathrm{i} + 2\,\zeta_s\eta - \mathrm{i}\right)\eta\sqrt{\epsilon_b} - \eta^4\mu_b + 2\mathrm{i}\zeta_s\left(\mu_b+1\right)\eta^3 \\ & + \left(\epsilon_b+1\right)\left(\mu_b+1\right)\eta^2 - 2\mathrm{i}\zeta_s\left(\mu_b+1\right)\epsilon_b\eta - \epsilon_b\left(\mu_b+1\right)\end{aligned} \tag{13}$$

where $\eta = \omega/\omega_s$.

*2.2. Structures isolated by inerter-based isolation systems*

In recent days, inerter based systems have been widely used for structural vibration control. The structure isolated by inerter-based isolation system is presented in Figure 1 (b).The equations of motion of the structure isolated by inerter-based isolation system [41] are expressed as:

$$\begin{aligned} m_s\ddot{y}_s + (m_s + m_{irb} + m_{in})\ddot{y}_{irb} + c_{irb}\dot{y}_{irb} + k_{irb}y_{irb} &= -(m_s + m_{irb})\ddot{u}_g \\ m_s\ddot{y}_s + c_s\dot{y}_s + k_s y_s &= -m_s(\ddot{u}_g + \ddot{y}_{irb}) \end{aligned} \tag{14}$$

Above equations of motion can be written as:

$$\begin{aligned} (\ddot{y}_s + \ddot{y}_{irb}) + 2\zeta\omega_s\dot{y}_s + \omega_s^2 y_s &= -\ddot{u}_g \\ (\ddot{y}_s + \ddot{y}_{irb}) + \mu_{irb}\ddot{y}_{irb} + \kappa^2\omega_s^2 y_{irb} + 2\xi\omega_s\dot{y}_{irb} + \mu\ddot{y}_{irb} &= -(1+\mu_{irb})\ddot{u}_g \end{aligned} \tag{15}$$

where mass ratio of base mass to structure: $\mu_{irb} = \frac{m_{irb}}{m_s}$, frequency of the structure: $\omega_s = \sqrt{\frac{k_s}{m_s}}$, viscous damping ratio of the structure: $\zeta = \frac{c_s}{2m_s\omega_s}$, frequency ratio of the inerter-bi to structure: $\kappa = \sqrt{\frac{k_{irb}}{m_s}}/\omega_s$, viscous damping ratio of the inerter-bi: $\xi = \frac{c_{irb}}{2\sqrt{k_s m_s}}$, mass ratio of inerter to structure: $\mu = \frac{m_{in}}{m_s}$. In Eq. (15), $y_{irb} = (u_{irb} - u_g)$, the relative displacement of the base mass with respect to ground and $y_s = (u_s - u_{irb})$, the relative displacement of structure with respect to base mass. It is considered that the isolated system is subjected to harmonic ground motions. The steady state solutions of the

displacements of the dynamic system isolated by Inerter-BI under harmonic ground motions can be evaluated as: $y_s = Y_s e^{\mathrm{i}\omega t}$, $y_{irb} = Y_{irb} e^{\mathrm{i}\omega t}$. $(\dot{\bullet})$ defines the derivative with respect to time. The function of ground accelerations are considered as $u_g = U_g e^{\mathrm{i}\omega t}$. The transfer function can be formed as:

$$\begin{bmatrix} V_{11} & V_{12} \\ V_{21} & V_{22} \end{bmatrix} \begin{Bmatrix} Y_s \\ Y_{irb} \end{Bmatrix} = -q^2 \begin{bmatrix} 1 \\ 1+\mu_{irb} \end{bmatrix} U_g \tag{16}$$

$$V_{11} = 2\,\zeta_s q\omega_s + q^2 + {\omega_s}^2; V_{12} = q^2; V_{21} = q^2; V_{22} = (1+\mu+\mu_{irb})\,q^2 + 2\,\xi\,q\omega_s + \kappa^2{\omega_s}^2 \tag{17}$$

where $q = \mathrm{i}\omega$. The displacement responses of structure and Inerter-BI are evaluated as:

$$H_s(q) = \frac{Y_s}{U_g} = \frac{-q^2(\kappa^2{\omega_s}^2 + \mu\,q^2 + 2\,\xi\,q\omega_s)}{\Delta_{irb}} \tag{18}$$

$$H_{irb}(q) = \frac{Y_{irb}}{U_g} = \frac{-q^2\left(\ 2\,\zeta\,q\mu_{irb}\omega_s + 2\,\zeta\,q\omega_s + q^2\mu_{irb} + \mu_{irb}{\omega_s}^2 + {\omega_s}^2\ \right)}{\Delta_{irb}} \tag{19}$$

$$\begin{aligned} \Delta_{irb} = {} & (\mu+\mu_{irb})\,q^4 + 2\,\left((1+\mu+\mu_{irb})\,\zeta + \xi\right)\omega_s q^3 + \kappa^2{\omega_s}^4 \\ & + {\omega_s}^2\left(4\,\zeta\,\xi + \kappa^2 + \mu + \mu_{irb} + 1\right)q^2 + 2\,{\omega_s}^3\left(\zeta\,\kappa^2 + \xi\right)q \end{aligned} \tag{20}$$

The shear force can be obtained as:

$$H_{sf}(q) = \frac{q\zeta Y_s + \omega_s^2 Y_s}{U_g} = \frac{\left(\ -q^2(\kappa^2{\omega_s}^2 + \mu\,q^2 + 2\,\xi\,q\omega_s)\left(q\zeta + {\omega_s}^2\right)\ \right)}{\Delta_{irb}} \tag{21}$$

The displacement responses of the structure can also be evaluated in non-dimensional manner. To evaluate the dimensionless responses, Eq. (16) can be re-constructed as:

$$\begin{bmatrix} \tilde{V}_{11} & \tilde{V}_{12} \\ \tilde{V}_{21} & \tilde{V}_{22} \end{bmatrix} \begin{Bmatrix} Y_s \\ Y_{irb} \end{Bmatrix} = \eta^2 \begin{bmatrix} 1 \\ 1+\mu_{irb} \end{bmatrix} U_g \tag{22}$$

$$\tilde{V}_{11} = -\eta^2 + 2\mathrm{i}\zeta\,\eta + 1; \tilde{V}_{12} = -\eta^2; \tilde{V}_{21} = -\eta^2; \tilde{V}_{22} = -\left(1+\mu+\mu_{irb}\right)\eta^2 + 2\mathrm{i}\xi\,\eta + \kappa^2 \tag{23}$$

The displacement responses of the structure and Inerter-BI are evaluated as:

$$H_s(\eta) = \frac{Y_s}{U_g} = \frac{-\eta^2(-\eta^2\mu + \kappa^2 + 2\mathrm{i}\xi\,\eta)}{\Delta_{irb}} \tag{24}$$

$$H_{irb}(\eta) = \frac{Y_{irb}}{U_g} = \frac{-\eta^2\left(\ -\eta^2\mu_{irb} + \mu_{irb} + 1 + 2\mathrm{i}\zeta\,\eta\,\left(1+\mu_{irb)}\right)\ \right)}{\Delta_{irb}} \tag{25}$$

$$\begin{aligned} \Delta_{irb} = {} & -\eta^4\mu - \eta^4\mu_{irb} + 4\,\zeta\,\eta^2\xi + \eta^2\kappa^2 + \eta^2\mu + \eta^2\mu_{irb} \\ & + \eta^2 - \kappa^2 + 2\mathrm{i}\left(\left(\left(\mu+\mu_{irb}+1\right)\zeta + \xi\right)\eta^2 - \zeta\,\kappa^2 - \xi\right)\eta \end{aligned} \tag{26}$$

*2.3. Structures isolated by inertial amplifier coupled base isolators*

The schematic diagram and free body diagrams of inertial amplifier are presented Figure 2.

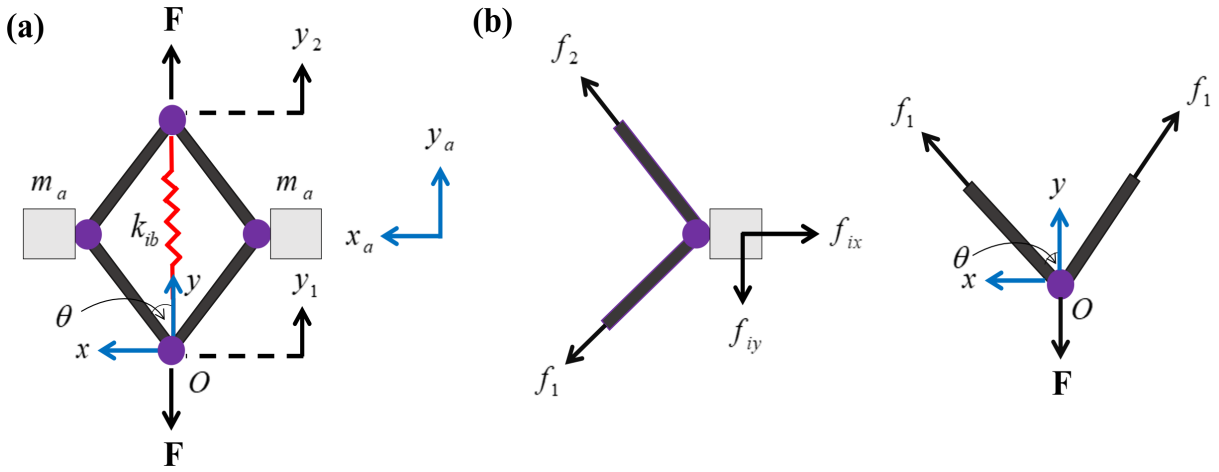


**Figure** 2: (a) Schematic diagram of inertial amplifier (b) free-body diagram of inertial amplifier.

An inertial angle $\theta$ between the y-axis and bars, is indicated in the diagrams when the inertial amplifier is in undeformed state. It is considered that the system moves towards the y-axis and small deflections occurred in lateral masses in x and y-directions. $x_a$ and $y_a$ indicate the displacement of lateral masses in x and y-directions, respectively. The values of the deflections can be evaluated as:

$$y_a = \frac{y_1 + y_2}{2} \tag{27}$$

$$x_a = \pm\frac{y_2 - y_1}{2\tan\theta} \tag{28}$$

It is assumed the total system is in equilibrium condition and inertial forces generated through the lateral masses can be evaluated as: $f_{ix} = m\ddot{x}_a$ and $f_{iy} = m\ddot{y}_a$. The internal forces through the rigid links are obtained as $f_1$ and $f_2$ and presented in Figure 2 (b). The values of $f_1$ and $f_2$ can be evaluated as:

$$f_1 = \frac{1}{2}\left(\frac{f_{ix}}{\sin\theta} - \frac{f_{iy}}{\cos\theta}\right) \tag{29}$$

$$f_2 = \frac{1}{2}\left(\frac{f_{ix}}{\sin\theta} + \frac{f_{iy}}{\cos\theta}\right) \tag{30}$$

The total reaction forces through the system presented in Figure 2 can be evaluated as:

$$\begin{aligned} F &= -2f_1\cos\theta + k_{ib}(y_2 - y_1) \\ &= d_1\left(\ddot{y}_2 - \ddot{y}_1\right) + d_2\left(\ddot{y}_2 + \ddot{y}_1\right) + k_{ib}(y_2 - y_1) \end{aligned} \tag{31}$$

in which $d_1 = \frac{0.5m_a}{\tan^2\theta}$ and $d_2 = 0.5m_a$ are the constants produced through the balancing of the inertial forces generated in the inertial amplifier which is presented in Figure 2 (a). In the lateral masses, the total inertial forces are proportional to the mean of accelerations $\left(\frac{\ddot{y}_2+\ddot{y}_1}{2}\right)$ generated through the two terminals of the inertial amplifier and the inertial constant $d_2$ is produced through that. $d_1$ constant produced by the inertial forces generated in the geometry of the inertial amplifier and the lateral masses of the entire system. It is observed that the inertial forces of the entire system is directly proportional to the relative acceleration $\left(\frac{\ddot{y}_2-\ddot{y}_1}{2}\right)$ between two terminals. The equations of motion of the structure isolated by inertial amplifier coupled base isolator in Figure 1 (c) can be obtained as:

$$\begin{aligned} m_{ia}\ddot{y}_{ib} + c_{ib}\dot{y}_{ib} + k_{ib}y_{ib} - k_s y_s - c_s\dot{y}_s &= -m_{ia}\ddot{u}_g \\ m_s\ddot{y}_s + m_s\ddot{y}_{ib} + c_s\dot{y}_s + k_s y_s &= -m_s\ddot{u}_g \end{aligned} \tag{32}$$

In Eq. (32), the total effective mass of the IABI is evaluated as: $m_{ia} = m_{ib} + 0.5m_a\left(1 + \frac{1}{\tan^2\theta}\right)$. Now, inertial amplification need to be evaluated and can be determined as:

$$\alpha = \frac{m_a}{m_{ib} + 2m_a}; m_a = \left(\frac{\alpha}{(1-2\alpha)}\right) m_{ib} \tag{33}$$

$$\beta = \frac{m_{ib}}{m_{ib} + 2m_a} = (1 - 2\alpha) \tag{34}$$

$$\Lambda_f = \frac{m_{ib}}{m_{ib} + 2m_a} + \frac{0.5m_a}{m_{ib} + 2m_a}\left(1 + \frac{1}{\tan^2\theta}\right) = (1 - 1.5\alpha) + \left(\frac{0.5\alpha}{\tan^2\theta}\right) \tag{35}$$

In Eq. (33), Eq. (34), and Eq. (35), $\alpha$, $\beta$, and $\Lambda_f$ refer the mass ratios of inertial amplifier, base mass, and effective mass to the total static mass of the IABI. The inertial amplification of IABI system is presented in Figure 3.

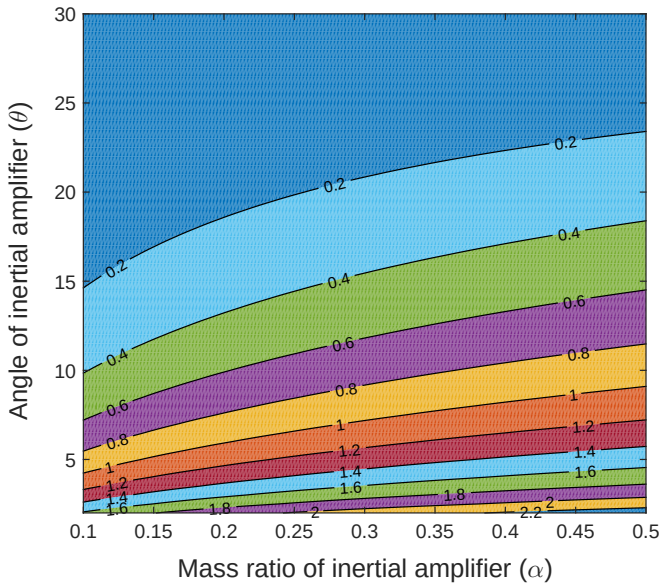


**Figure** 3: Contours of $log_{10}$ of inertial amplification of IABI as a function of the inertial angle $\theta$ and mass ratio $\alpha$.

In Figure 3, more inertial amplification occurs at the lower angel and higher mass ratio of the inertial amplifier to total static mass $\alpha$. To get inertial amplification through the increment of dynamic mass, $\alpha < 0.5$. At $\alpha = 0.5$, the effective mass ratio $\Lambda_f = 0$ and $\alpha > 0.5$, the effective mass ratio $\Lambda_f$ becomes $-ve$. In Eq. (32), the relative displacement of base with respect to ground: $y_{ib} = (u_{ib} - u_g)$, and the relative displacement of structure with respect to base mass: $y_s = (u_s - u_{ib})$. It is considered that the isolated system is subjected to harmonic ground motions. The steady state solutions of the displacements of the dynamic system isolated by IABI under harmonic ground motions can be evaluated as: $y_s = Y_s e^{\mathrm{i}\omega t}$, $y_{ib} = Y_{ib} e^{\mathrm{i}\omega t}$. $(\dot{\bullet})$ defines the derivative with respect to time. The function of ground accelerations are considered as $u_g = U_g e^{\mathrm{i}\omega t}$. The displacement of the structure and IABI can be obtained by deriving the solutions analytically. After substituting the steady state solutions in Eq. (32), the transfer matrix can be formed. From where the responses can be evaluated easily and the transfer matrix of the above equations motion can be presented as:

$$\begin{bmatrix} B_{11} & B_{12} \\ B_{21} & B_{22} \end{bmatrix} \begin{Bmatrix} Y_s \\ Y_{ib} \end{Bmatrix} = -q^2 \begin{bmatrix} 1 \\ \mu_{ia} \end{bmatrix} U_g \tag{36}$$

$$B_{11} = 2\,\zeta_s q\omega_s + q^2 + {\omega_s}^2; B_{12} = q^2; B_{21} = -2\,\zeta_s q\omega_s - {\omega_s}^2 B_{22} = 2\,\zeta_{ib} q\omega_{ib}\mu_{ia} + \mu_{ia} q^2 + {\omega_{ib}}^2\mu_{ia} \tag{37}$$

where $q = \mathrm{i}\omega$. The displacement responses of structure and IABI are evaluated as:

$$H_s(q) = \frac{Y_s}{U_g} = \frac{-q^2\mu_{ia}\omega_{ib}\,(2\,\zeta_{ib} q + \omega_{ib})}{\Delta_{ia}} \tag{38}$$

$$H_{ib}(q) = \frac{Y_{ib}}{U_g} = \frac{-q^2\,(\;2\,q\zeta_s\mu_{ia}\omega_s + \mu_{ia} q^2 + 2\,\zeta_s q\omega_s + \mu_{ia}{\omega_s}^2 + {\omega_s}^2\;)}{\Delta_{ia}} \tag{39}$$

$$\Delta_{ia} = q^4\mu_{ia} + \left(\left(2\,\zeta_{ib}\omega_{ib} + 2\,\zeta_s\omega_s\right)\mu_{ia} + 2\,\zeta_s\omega_s\right)q^3 + \left(\left(4\,\zeta_{ib}\zeta_s\omega_{ib}\omega_s + {\omega_{ib}}^2 + {\omega_s}^2\right)\mu_{ia} + {\omega_s}^2\right)q^2 + 2\,\mu_{ia}\omega_s\omega_{ib}\left(\zeta_{ib}\omega_s + \zeta_s\omega_{ib}\right)q + \mu_{ia}{\omega_{ib}}^2{\omega_s}^2 \tag{40}$$

The shear force can be obtained as:

$$H_{sf}(q) = \frac{q\zeta_s Y_s + \omega_s^2 Y_s}{U_g} = \frac{\left(\ -q^2\mu_{ia}\omega_{ib}\left(2\,\zeta_{ib}q + \omega_{ib}\right)\left(q\zeta_s + {\omega_s}^2\right)\ \right)}{\Delta_{ia}} \tag{41}$$

The displacement responses of the structure can also be evaluated in non-dimensional manner. To evaluate the dimensionless responses, Eq. (36) can be re-constructed as:

$$\begin{bmatrix} \tilde{B}_{11} & \tilde{B}_{12} \\ \tilde{B}_{21} & \tilde{B}_{22} \end{bmatrix} \begin{Bmatrix} Y_s \\ Y_{ib} \end{Bmatrix} = \eta^2 \begin{bmatrix} 1 \\ \mu_{ia} \end{bmatrix} U_g \tag{42}$$

$$\tilde{B}_{11} = -\eta^2 + 2\mathrm{i}\zeta_s\eta + 1; \tilde{B}_{12} = -\eta^2; \tilde{B}_{21} = -2\mathrm{i}\zeta_s\eta - 1; \tilde{B}_{22} = -\mu_{ia}\eta^2 + 2\mathrm{i}\zeta_{ib}\eta\,\eta_{ib}\mu_{ia} + {\eta_{ib}}^2\mu_{ia} \tag{43}$$

The displacement responses of the structure and IABI are evaluated as:

$$H_s(\eta) = \frac{Y_s}{U_g} = \frac{-\mu_{ia}\eta^2\eta_{ib}\left(2\mathrm{i}\zeta_{ib}\eta + \eta_{ib}\right)}{\Delta_{ib}} \tag{44}$$

$$H_{ib}(\eta) = \frac{Y_{ib}}{U_g} = \frac{-\eta^2\left(\ -\mu_{ia}\eta^2 + \mu_{ia} + 1 + 2\mathrm{i}\left(\eta\,\zeta_s\mu_{ia} + \zeta_s\eta\right)\ \right)}{\Delta_{ib}} \tag{45}$$

$$\Delta_{ib} = \left(-\eta^4 + \left(4\,\zeta_{ib}\zeta_s\eta_{ib} + {\eta_{ib}}^2 + 1\right)\eta^2 - {\eta_{ib}}^2\right)\mu_{ia} + \eta^2 + 2\,\mathrm{i}\eta\left(\left(\left(\eta_{ib}\zeta_{ib} + \zeta_s\right)\eta^2 - \zeta_s{\eta_{ib}}^2 - \eta_{ib}\zeta_{ib}\right)\mu_{ia} + \eta^2\zeta_s\right) \tag{46}$$

where frequency ratio of harmonic ground motions to structure: $\eta = \frac{\omega}{\omega_s}$, mass ratio of IABI to structure: $\mu_{ia} = \frac{m_{ia}}{m_s}$, frequency ratio of IABI to structure: $\eta_{ib} = \frac{\omega_{ib}}{\omega_s}$, viscous damping ratio of IABI: $\zeta_{ib} = \frac{c_{ib}}{2m_{ia}\omega_{ib}}$, and viscous damping ratios of the structure: $\zeta_s = \frac{c_s}{2m_s\omega_s}$, frequency of the structure: $\omega_s = \sqrt{\frac{k_s}{m_s}}$, frequency of the IABI: $\omega_{ib} = \sqrt{\frac{k_{ib}}{m_{ia}}}$.

## 3. Stochastic response evaluation

To evaluate the stochastic responses, it is considered that the isolated structures in Figure 1 are subjected to Gauassian White Noise. It is also noted that all the isolated structures are linear vibratory system and the general form of the equations of motion Eq. (1), Eq. (14) and Eq. (32) can be written as:

$$M\ddot{y}(t) + C\dot{y}(t) + Ky(t) = -F_b(t) \tag{47}$$

$F_b(t)$ represents the forcing vector which is different for each isolated structure and presented as: $[m_s, m_b]^T\ddot{u}_g(t)$ for structure isolated by CBI, $[m_s, (m_s{+}m_{irb})]^T\ddot{u}_g(t)$ for structure isolated by Inerter-BI, and $[m_s, m_{ia}]^T\ddot{u}_g(t)$ for structure isolated by IABI. Each force acting to the corresponding degree of freedom. The general form of the forcing function can be represented as:

$$F_b(t) = \begin{Bmatrix} f_{b1}(t) \\ f_{b2}(t) \\ \ldots \\ f_{bn}(t) \end{Bmatrix} \tag{48}$$

Each component of force $f_{bi}(t)$ is assumed as randomly correlated. The power spectral density matrix can be formed as:

$$S_{F_bF_b}(\omega) = E[F_b(\omega)^* F_b(\omega)] = \begin{bmatrix} S_{f_{b1}f_{b1}}(\omega) & S_{f_{b1}f_{b2}}(\omega) & \ldots & S_{f_{b1}f_{bn}}(\omega) \\ S_{f_{b2}f_{b1}}(\omega) & S_{f_{b2}f_{b2}}(\omega) & \ldots & S_{f_{b2}f_{bn}}(\omega) \\ \ldots & \ldots & \ldots & \ldots \\ S_{f_{bn}f_{b1}}(\omega) & S_{f_{bn}f_{b2}}(\omega) & \ldots & S_{f_{bn}f_{bn}}(\omega) \end{bmatrix} \tag{49}$$

In Eq. (49), the off-diagonal values are indicated as cross power spectral density functions and the diagonal values are indicated as auto power spectral density functions. After substituting $\ddot{u}_g(t) = U_g e^{\mathrm{i}\omega t}$ in $F_b(t)$, the loading function can be represented in frequency domain and presented as: $F_b(t) = F_b(\omega)e^{\mathrm{i}\omega t}$. In Eq. (47), $y(t)$ refers the displacement vectors containing the relative displacement of the main structure $y_s(t)$ and each isolator (i.e. $y_b(t)$ for CBI, $y_{irb}(t)$ for Inerter-BI, $y_{ib}(t)$ for IABI), respectively. Thus, the displacement vectors for each isolated system are represented as: $[y_s, y_b]^T$ for structure isolated by CBI, $[y_s, y_{irb}]^T$ for structure isolated by Inerter-BI, and $[y_s, y_{ib}]^T$ for structure isolated by IABI. The generalized form of the displacement response vectors can be converted to frequency domain by assuming $y(t) = Y(\omega)e^{\mathrm{i}\omega t}$, where $Y(\omega)$ is the displacement amplitude vectors of the isolated structures. After substituting the values of $y(t)$ and $F_b(t)$ in Eq. (47), the equations of motions are converted to frequency domain and presented as:

$$(q^2M + qC + K)Y(\omega) = -F_b(\omega); U(\omega)Y(\omega) = -F_b(\omega); Y(\omega) = H(\omega)F_b(\omega) \tag{50}$$

The matrix of power spectral density containing the vector $y(t)$ is obtained as:

$$S_{YY}(\omega) = E[Y(\omega)Y(\omega)^*] = H(\omega)S_{F_bF_b}(\omega)H(\omega)^* \tag{51}$$

The Gaussian White Noise have zero mean and standard deviation 2. The standard deviation of the displacement response has derived by using the dimensional terms to implement the formula below:

$$\sigma_{y_s}^2 = E[y_s^2(t)] = R_{yy}(0) = \int_{-\infty}^{\infty} |H(\omega)|^2 S_{F_bF_b}(\omega)\,\mathrm{d}\omega \tag{52}$$

In the frequency domain, the velocity of the structure can be expressed as

$$\dot{Y}_s(\omega) = (\mathrm{i}\omega)Y_s(\omega) = (\mathrm{i}\omega)H_s(\omega)F_b(\omega) \tag{53}$$

Since $\dot{y}_s(t)$ is also a zero-mean stationary Gaussian random process, its standard deviation can be obtained in a similar manner as

$$\sigma_{\dot{y}_s}^2 = E[\dot{y}_s^2(t)] = \int_{-\infty}^{\infty} \{(\mathrm{i}\omega)H(\omega)\}\{(\mathrm{i}\omega)H(\omega)\}^* S_{F_bF_b}(\omega)\mathrm{d}\omega = \int_{-\infty}^{\infty} \omega^2 |H_s(\omega)|^2 S_{F_bF_b}(\omega)\mathrm{d}\omega \tag{54}$$

The expressions of $\sigma_{y_s}$ and $\sigma_{\dot{y}_s}$ are then substituted into the expressions derived in the previous subsections. The calculation of the integral on the right-hand side of equations Eq. (52) and Eq. (54) in general requires the calculation of integrals involving the ratio of polynomials of the following form

$$I_n = \int_{-\infty}^{\infty} \frac{\Xi_n(\omega)\,\mathrm{d}\omega}{\Lambda_n(\mathrm{i}\omega)\Lambda_n^*(\mathrm{i}\omega)} \tag{55}$$

$(\bullet)^*$complex conjugate. Here the polynomials are expressed as

$$\Xi_n(\omega) = b_{n-1}\omega^{2n-2} + b_{n-2}\omega^{2n-4} + \cdots + b_0 \tag{56}$$

$$\Lambda_n(\mathrm{i}\omega) = a_n(\mathrm{i}\omega)^n + a_{n-1}(\mathrm{i}\omega)^{n-1} + \cdots + a_0 \tag{57}$$

Following Roberts and Spanos [69]this integral can be evaluated as

$$I_n = \frac{\pi}{a_n}\frac{\det[\mathbf{N}_n]}{\det[\mathbf{D}_n]}. \tag{58}$$

Here the $n \times n$ matrices are defined as

$$\mathbf{N}_n = \begin{bmatrix} b_{n-1} & b_{n-2} & & \cdots & & & b_0 \\ -a_n & a_{n-2} & -a_{n-4} & a_{n-6} & \cdots & 0 & \cdots \\ 0 & -a_{n-1} & a_{n-3} & -a_{n-5} & \cdots & 0 & \cdots \\ 0 & a_n & -a_{n-2} & a_{n-4} & \cdots & 0 & \cdots \\ 0 & \cdots & & & \cdots & 0 & \cdots \\ 0 & 0 & & & \cdots & -a_2 & a_0 \end{bmatrix} \tag{59}$$

and

$$\mathbf{D}_n = \begin{bmatrix} a_{n-1} & -a_{n-3} & a_{n-5} & -a_{n-7} & & & \\ -a_n & a_{n-2} & -a_{n-4} & a_{n-6} & \cdots & 0 & \cdots \\ 0 & -a_{n-1} & a_{n-3} & -a_{n-5} & \cdots & 0 & \cdots \\ 0 & a_n & -a_{n-2} & a_{n-4} & \cdots & 0 & \cdots \\ 0 & \cdots & & & \cdots & 0 & \cdots \\ 0 & 0 & & & \cdots & -a_2 & a_0 \end{bmatrix} \tag{60}$$

These expressions will be used for the two cases considered. We assume that the excitation $\ddot{u}_g$ is Gaussian white noise so that its spectral density is constant with respect to frequency. But different spectral densities can be easily used within the scope of this formulation.

*3.1. Peak statistics for structure with inertial amplifier coupled base isolator*

Since the forcing function has constant spectral density we assume that

$$S_{F_b F_b}(\omega) = S_0 \tag{61}$$

As the input spectrum is considered as white, thus $S_0$ refers a constant for all frequencies. Therefore, the standard deviation of $y_s(t)$ can be obtained using equation Eq. (52) as

$$\sigma_{y_s}^2 = \int_{-\infty}^{\infty} |H(\omega)|^2 S_0 \, \mathrm{d}\omega = S_0 \int_{-\infty}^{\infty} \frac{\omega^2}{\Delta_1(\mathrm{i}\omega)\Delta_1^*(\mathrm{i}\omega)} \, \mathrm{d}\omega \tag{62}$$

The standard deviation of the derivative of the voltage $\dot{y_s}(t)$ can be obtained using equation Eq. (54) as

$$\sigma_{\dot{y}_s}^2 = \int_{-\infty}^{\infty} \omega^2 |H(\omega)|^2 S_0 \, \mathrm{d}\omega = S_0 \int_{-\infty}^{\infty} \frac{\omega^4}{\Delta_1(\mathrm{i}\omega)\Delta_1^*(\mathrm{i}\omega)} \, \mathrm{d}\omega \tag{63}$$

The shear force of the structure due to the effect of random ground motions can be evaluated as:

$$\sigma_{sf}^2 = \int_{-\infty}^{\infty} |H_{sf}(\omega)|^2 S_0 \, \mathrm{d}\omega \tag{64}$$

It can be found from the Eq. (65) that it is a $4^{th}$ order polynomial equation.

$$\begin{aligned} \Delta_{ia} = q^4 \mu_{ia} + \left( \left( 2\,\zeta_{ib}\omega_{ib} + 2\,\zeta_s\omega_s \right) \mu_{ia} + 2\,\zeta_s\omega_s \right) q^3 + \left( \left( 4\,\zeta_{ib}\zeta_s\omega_{ib}\omega_s + {\omega_{ib}}^2 + {\omega_s}^2 \right) \mu_{ia} + {\omega_s}^2 \right) q^2 + \\ 2\,\mu_{ia}\omega_s\omega_{ib} \left( \zeta_{ib}\omega_s + \zeta_s\omega_{ib} \right) q + \mu_{ia}{\omega_{ib}}^2{\omega_s}^2 \end{aligned} \tag{65}$$

where $q = \mathrm{i}\omega$. The solution is derived below:

$$\begin{aligned} n = 4, b_0 = 0, b_1 = 0, b_2 = 1, b_3 = 0, a_0 = \mu_{ia}{\omega_{ib}}^2{\omega_s}^2, a_1 = 2\,\mu_{ia}\omega_s\omega_{ib} \left( \zeta_{ib}\omega_s + \zeta_s\omega_{ib} \right), \\ a_2 = \left( 4\,\zeta_{ib}\zeta_s\omega_{ib}\omega_s + {\omega_{ib}}^2 + {\omega_s}^2 \right) \mu_{ia} + {\omega_s}^2, a_3 = \left( 2\,\zeta_{ib}\omega_{ib} + 2\,\zeta_s\omega_s \right) \mu_{ia} + 2\,\zeta_s\omega_s, a_4 = \mu_{ia} \end{aligned} \tag{66}$$

Now using Eq. (55), the integral can be evaluated as

$$\int_{-\infty}^{\infty} \frac{\omega^2}{\Delta(\mathrm{i}\omega)\Delta^*(\mathrm{i}\omega)} \mathrm{d}\omega = \frac{\pi}{a_4} \frac{\det \begin{bmatrix} b_3 & b_2 & b_1 & 0 \\ -a_4 & a_2 & -a_0 & 0 \\ 0 & -a_3 & a_1 & 0 \\ 0 & -a_4 & a_2 & a_0 \end{bmatrix}}{\det \begin{bmatrix} a_3 & -a_1 & 0 & 0 \\ -a_4 & a_2 & -a_0 & 0 \\ 0 & -a_3 & a_1 & 0 \\ 0 & -a_4 & a_2 & a_0 \end{bmatrix}} \tag{67}$$

The standard deviation of the displacement response due to white represented as:

$$\sigma_{y_s}^2 = \frac{S_0 \pi \left( \zeta_{ib}\omega_s + \zeta_s\omega_{ib} \right)}{\left( \begin{array}{c} 8\,{\zeta_{ib}}^3\zeta_s\mu_{ia}{\omega_{ib}}^2{\omega_s}^2 + 8\,\omega_{ib}\mu_{ia}\omega_s \left( \left( 0.25 + \left( \mu_{ia} + 1 \right) {\zeta_s}^2 \right) {\omega_s}^2 + \mu_{ia}{\zeta_s}^2{\omega_{ib}}^2 \right) \zeta_{ib}{}^2 \\ +8\,\zeta_s \left( 0.25\,{\left( \mu_{ia} + 1 \right)}^2 {\omega_s}^4 + {\omega_{ib}}^2 \left( \left( \mu_{ia} + 1 \right) {\zeta_s}^2 - 0.5\,\mu_{ia} \right) \mu_{ia}{\omega_s}^2 + 0.25\,{\mu_{ia}}^2{\omega_{ib}}^4 \right) \zeta_{ib} \\ +2\,{\zeta_s}^2\mu_{ia}{\omega_{ib}}^3\omega_s \end{array} \right)} \tag{68}$$

The standard deviation in velocity responses are derived as:

$$\sigma_{\dot{y}_s}^2 = \frac{S_0 4\,\pi\,\left(\,\left(\,{\zeta_s}^2\zeta_{ib}\omega_s{\omega_{ib}}^2+\zeta_s{\zeta_{ib}}^2{\omega_s}^2\omega_{ib}+0.25\,\zeta_s{\omega_{ib}}^3+0.25\,\zeta_{ib}{\omega_s}^3\,\right)\mu_{ia}+0.25\,\zeta_{ib}{\omega_s}^3\,\right)}{8\,\mu_{ia}\left(\begin{array}{c}\zeta_s\zeta_{ib}\left(\begin{array}{c}{\zeta_{ib}}^2{\omega_s}^2{\omega_{ib}}^2+\zeta_s\omega_s\omega_{ib}\left({\omega_{ib}}^2+{\omega_s}^2\right)\zeta_{ib}\\+0.25\,{\omega_s}^4+{\omega_{ib}}^2\left({\zeta_s}^2-0.5\right){\omega_s}^2+0.25\,{\omega_{ib}}^4\end{array}\right){\mu_{ia}}^2\\+\left(\begin{array}{c}{\omega_s}^2\omega_{ib}\left(0.25+{\zeta_s}^2\right){\zeta_{ib}}^2+0.25\,{\zeta_s}^2{\omega_{ib}}^3\\+\zeta_s\omega_s\left({\zeta_s}^2{\omega_{ib}}^2+0.5\,{\omega_s}^2\right)\zeta_{ib}\end{array}\right)\omega_s\mu_{ia}+0.25\,\zeta_s\zeta_{ib}{\omega_s}^4\end{array}\right)} \tag{69}$$

The standard deviation values for the shear force can be evaluated in similar manner. Now considered, $\zeta_s = 0$, and the mean square values are evaluated as:

$$\sigma_{y_s}^2 = \frac{S_0\pi}{2\zeta_{ib}{\omega_s}^2\omega_{ib}\mu_{ia}} = \frac{S_0\pi}{2{\omega_s}^3\zeta_{ib}\eta_{ib}\mu_{ia}} \tag{70}$$

$$\sigma_{\dot{y}_s}^2 = \frac{\left(\mu_{ia}+1\right)S_0\pi}{2\zeta_{ib}{\mu_{ia}}^2\omega_{ib}} = \frac{\left(\mu_{ia}+1\right)S_0\pi}{2\omega_s\zeta_{ib}{\mu_{ia}}^2\eta_{ib}} \tag{71}$$

Shear force can be evaluated as:

$$\sigma_{sf}^2 = \frac{S_0\pi\,\left({\omega_s}^2+\omega_{ib}\right)}{8\,{\omega_s}^4\zeta_{ib}\Delta_{sf}} \tag{72}$$

$$\Delta_{sf} = \left(\begin{array}{c}\left(\frac{1}{4}+\frac{{\mu_{ia}}^2}{4}+\left(\frac{\omega_{ib}}{4}+\frac{1}{2}\right)\mu_{ia}\right){\omega_s}^8+\left(\left({\zeta_{ib}}^2-\frac{\omega_{ib}}{4}\right)\mu_{ia}+{\zeta_{ib}}^2+\frac{\omega_{ib}}{4}\right)\mu_{ia}\omega_{ib}{\omega_s}^6\\+\frac{\left(4\,{\zeta_{ib}}^4+\left(-\omega_{ib}+2\right){\zeta_{ib}}^2-\omega_{ib}\right)\mu_{ia}}{4}+\frac{{\zeta_{ib}}^2}{2}+{\zeta_{ib}}^2{\mu_{ia}}^2{\omega_{ib}}^3\left({\zeta_{ib}}^2-\frac{\omega_{ib}}{4}\right){\omega_s}^2+\frac{{\zeta_{ib}}^4{\mu_{ia}}^2{\omega_{ib}}^4}{4}\end{array}\right) \tag{73}$$

It has observed that from Eq. (70) that the mass response of the structure is decreased by increasing the mass of the amplifier $m_{ia}$. Similar phenomena can also be observed damping ratio of the isolator $\zeta_{ib}$. Here uncertainties in the base excitation is considered. There can be uncertainties in the model parameters also. Under certain assumptions, the response statistics of SDOF uncertain systems can be obtained analytically [70, 71]. Future work will address the combined effect of model and base excitation uncertainties.

### *3.2. Comparison of stochastic responses of uncontrolled and controlled structures*

The stochastic responses of uncontrolled and controlled structures are evaluated under Gaussian White Noise. The parameters of the main structures are considered exactly same and total mass ratios, viscous damping ratios, and frequency ratios are also considered exactly same.

## 4. Stochastic and frequency domain responses

In this section, the seismic responses of controlled and uncontrolled structures subjected to harmonic and Gaussian White Noise are presented.

### *4.1. Comparison of seismic performance of CBI, Inerter-BI, and IABI under harmonic ground motions and Gaussian White Noise*

It is also noted that the super-structural parameters for uncontrolled and controlled structures are considered exactly same. The cumulative masses of classical base isolator, inerter-based isolator, and inertial amplifier coupled base isolator are remained similar as to compare between the seismic performance of the proposed isolation system and other conventional systems, respectively. Total system parameters of uncontrolled and controlled structures [41] are presented in Table 1.

**Table** 1: Details of system parameters of uncontrolled and controlled structures.

| Description | Symbol | | | Value |
|---|---|---|---|---|
| | CBI | Inerter-BI | IABI | |
| Structural damping ratio | $\zeta_s$ | $\zeta$ | $\zeta_s$ | 0.01 |
| Isolator damping ratio | $\zeta_b$ | $\xi$ | $\zeta_{ib}$ | 0.05 |
| Frequency ratio of isolator to structure | $\epsilon_b$ | $\kappa$ | $\eta_{ib}$ | 0.20 |
| Total mass ratio of isolator to structure | $\mu_b$ | $\mu_{irb}+\mu$ | $\mu_{ib}+2\mu_a$ | 0.6 |
| mass ratio of base mass to structure | ... | $\mu_{irb}$ | $\mu_{ib}$ | 0.4 |
| mass ratio of inerter to structure | ... | $\mu$ | ... | 0.2 |
| mass ratio of lateral mass to structure | ... | ... | $\mu_a$ | 0.1 |
| Inertial angle | ... | ... | $\theta$ | $30^o$ |

The dynamic response of isolated structures under harmonic ground motions are shown in Figure 4.

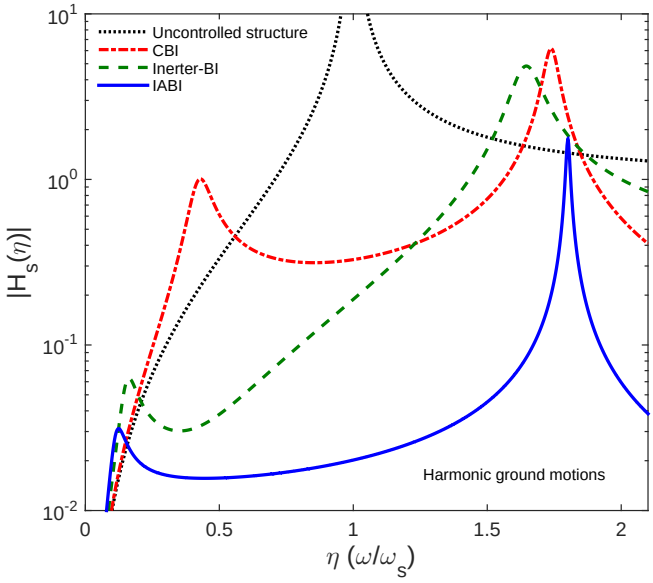


**Figure** 4: (a) Variations of displacement amplitudes of structures with frequency ratios.

In Figure 4(a), the displacement amplitudes of the uncontrolled structure, structure isolated by classical base isolation system, structure controlled by inerter-based isolation system, and structure with inertial amplifier coupled base isolator are compared. The peak non-dimensional displacement amplitudes of the structure isolated by CBI, Inerter-BI and IABI are evaluated as 6.17, 4.84 and 1.76. Thus, It is observed that the seismic performance of IABI system is significantly 71.47% and 63.60% superior to the CBI and Inerter-BI. The stochastic responses of the structure isolated by CBI and IABI are evaluated and presented in Figure 5.

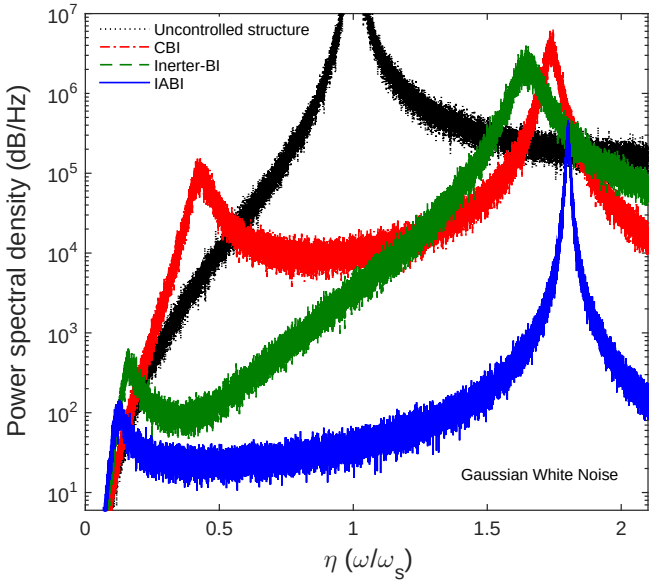


**Figure** 5: Variations of power spectral density of the structures with frequency ratios.

As the uncontrolled and controlled structures are linear, it is expected that the stochastic response behaviour is also similar to the harmonic responses.

*4.2. Sensitivity of system parameters of proposed IABI on the structural responses*

The dynamic responses of structure isolated by proposed IABI under harmonic ground motions for different values of $\zeta_{ib}$ are presented in Figure 6.

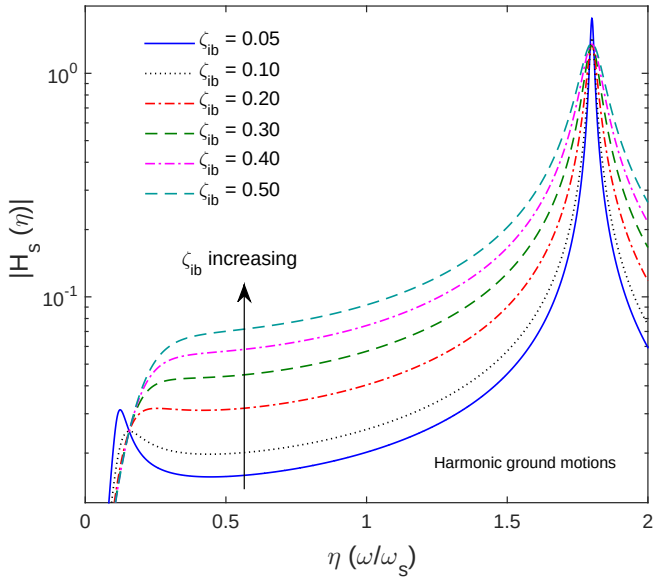


**Figure** 6: Variations of displacement amplitudes of the structures isolated by IABI with frequency ratio for different value of $\zeta_{ib}$, subjected to harmonic base excitation.

It can be observed from Figure 6 that for damping ratios less than 20% the peak displacement amplitude decreases, and it becomes pretty stable and approximately constant for higher damping values. The values of peak displacement amplitude of structure isolated by IABI are evaluated as 1.76, 1.44, 1.33, 1.34, 1.35, 1.36 for $0.05 < \zeta_{ib} < 0.50$.

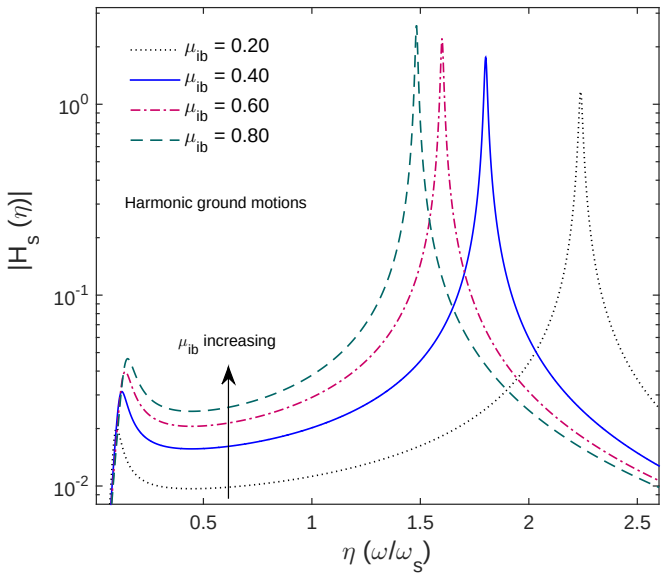


**Figure** 7: Variations of displacement amplitudes of the structures isolated by IABI with frequency ratio for different value of $\mu_{ib}$, subjected to harmonic base excitation.

In Figure 7, the displacement amplitudes of the structure isolated by IABIs for different values of the $\mu_{ib}$ are shown. The value of $\mu_{ib}$ are varied from 0.2 to 0.8. For the harmonic case, the peak values of the displacement amplitudes are as: 1.16, 1.76, 2.21, and 2.58. Similar type of results are observed for the random case. The seismic responses of the structures for different values of $\theta$ are presented in Figure 8.

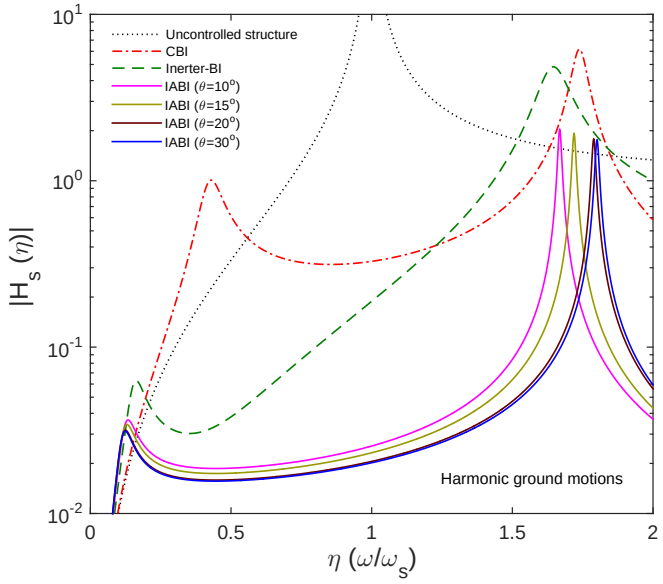


**Figure** 8: Variations of displacement amplitudes of the structures isolated by IABI with frequency ratio for different value of $\theta$, subjected to harmonic base excitation.

The structural displacement amplitudes are obtained for four different values of inertial angle $\theta$. $10^o$, $15^o$, $20^o$ and $30^o$ of the inertial angles are chosen to plot the results. For the harmonic case, the peak responses for adopted angles are 2.03, 1.92, 1.78, and 1.76. The stochastic response behaviour are also similar as all the systems are linear.

## 5. Time history analysis

The numerical study is conducted to evaluate the vibration reduction capacity of the proposed IABI. To perform the study, the time history plots of the uncontrolled and controlled structures are determined, and the structural responses of the controlled systems are compared with the structural responses of the uncontrolled structures. The masses of the structures ($m_s$) for uncontrolled and controlled structures are similar and considered as: 300 tons. Other structural and system parameters are already mentioned in the previous section. For the loading part, twenty-two real earthquake ground motions are implemented to perform these numerical study and the data of the earthquakes are downloaded from https://peer.berkeley.edu/peer-strong-ground-motion-databases. The details of the considered earthquakes are listed in Table 2. $E_s$ defines the epicentral distance in km.

**Table** 2: Details of earthquake ground motions.

| Earthquake | Year | $M_w$ | Recording station | $Vs_{30}$(m/s) | Component | $E_s$ (km) | PGA,g |
|---|---|---|---|---|---|---|---|
| Northridge | 1994 | 6.7 | Beverly Hills - Mulhol | 356 | MUL009 | 13.3 | 0.52 |
| Northridge | 1994 | 6.7 | Canyon Country-WLC | 309 | LOS270 | 26.5 | 0.48 |
| Duzce, Turkey | 1999 | 7.1 | Bolu | 326 | BOL090 | 41.3 | 0.82 |
| Hector Mine | 1999 | 7.1 | Hector | 685 | HEC000 | 26.5 | 0.34 |
| Imperial Valley | 1979 | 6.5 | Delta | 275 | H-DLT352 | 33.7 | 0.35 |
| Imperial Valley | 1979 | 6.5 | El Centro Array 11 | 196 | H-E11230 | 29.4 | 0.38 |
| Kobe, Japan | 1995 | 6.9 | Nishi-Akashi | 609 | NIS090 | 8.7 | 0.51 |
| Kobe, Japan | 1995 | 7.5 | Shin-Osaka | 256 | SHI000 | 46 | 0.24 |
| Kocaeli, Turkey | 1999 | 7.5 | Duzce | 276 | DZC270 | 98.2 | 0.36 |
| Kocaeli, Turkey | 1999 | 7.3 | Arcelik | 523 | ARC000 | 53.7 | 0.22 |
| Landers | 1992 | 7.3 | Yermo Fire Station | 354 | YER270 | 86 | 0.24 |
| Landers | 1992 | 7.3 | Coolwater | 271 | CLW-TR | 82.1 | 0.42 |
| Loma Prieta | 1989 | 6.9 | Capitola | 289 | CAP090 | 9.8 | 0.53 |
| Loma Prieta | 1989 | 6.9 | Gilroy Array 3 | 350 | G03000 | 31.4 | 0.56 |
| Manjil, Iran | 1990 | 7.4 | Abbar | 724 | ABBAR–T | 40.4 | 0.51 |
| Superstition Hills | 1987 | 6.5 | El Centro Imp. Co. | 192 | B-ICC090 | 35.8 | 0.36 |
| Superstition Hills | 1987 | 6.5 | Poe Road (temp) | 208 | B-POE270 | 11.2 | 0.45 |
| Cape Mendocino | 1992 | 7.0 | Rio Dell Overpass | 312 | RIO270 | 22.7 | 0.55 |
| Chi-Chi, Taiwan | 1999 | 7.6 | CHY101 | 259 | CHY101-N | 32 | 0.44 |
| Chi-Chi, Taiwan | 1999 | 7.6 | TCU045 | 705 | TCU045-N | 77.5 | 0.51 |
| San Fernando | 1971 | 6.6 | LA - Hollywood Stor | 316 | PEL180 | 39.5 | 0.21 |
| Friuli, Italy | 1976 | 6.5 | Tolmezzo | 425 | A-TMZ270 | 20.2 | 0.35 |

The response spectra[72] at 5% damping for all the selected records have been plotted and presented in Figure 9.

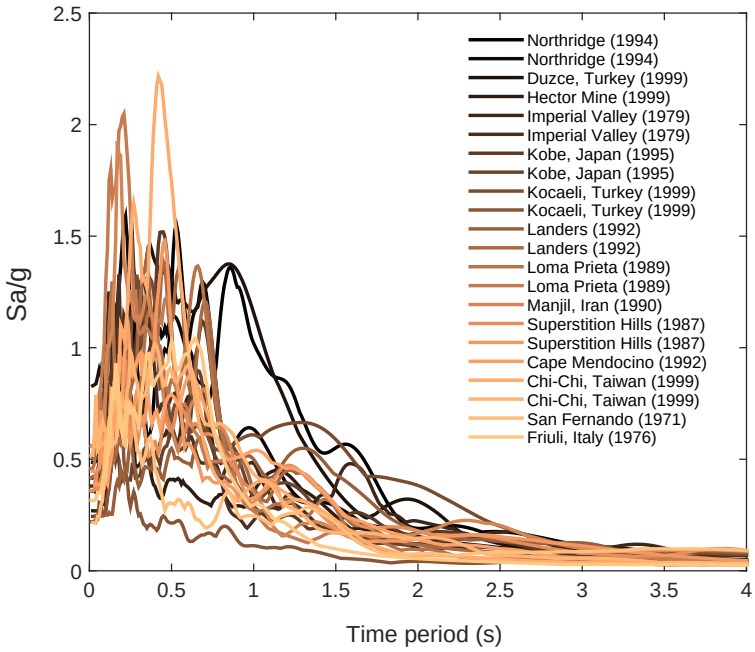


**Figure** 9: Response spectra of the various earthquakes considered along with the designed spectra.

The displacement histories of uncontrolled and controlled structures are presented in Figure 10.

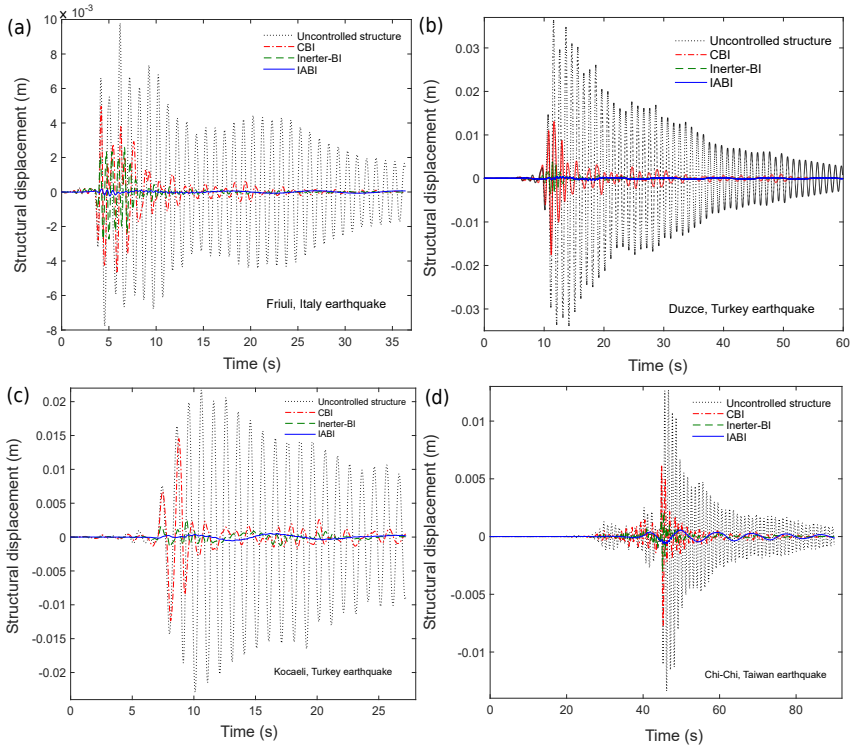


**Figure** 10: Displacement history of the structures with time for different earthquake ground motion.

The time history responses are evaluated for all twenty two earthquakes but only for plots are presented as the nature of the plots are similar. In Figure 11, statistical data of the displacement reduction (%) capacity of the proposed inertial amplifier coupled base isolator and classical base isolation is shown by

histogram plot.

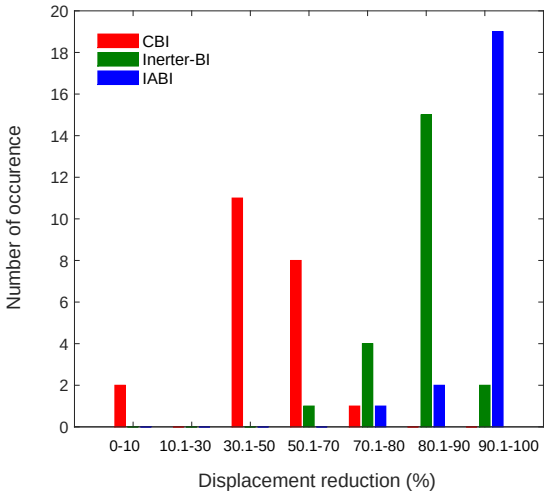


**Figure** 11: Variation of number of occurrence with range of displacement reduction percentage.

This plot provides the exact seismic performance of the IABI and CBI systems. The peak relative displacement of the structure for all structural systems along with the response reduction(%) is listed in Table 3.

**Table** 3: Displacement reduction (%) of structure with respect to uncontrolled structure under different earthquake ground motions.

| **Earthquake** | **Displacement reduction (%)** | | |
|---|---|---|---|
| | **CBI** | **Inerter-BI** | **IABI** |
| Northridge | 61.86 | 92.33 | 99.04 |
| Northridge | 56.48 | 86.57 | 98.76 |
| Duzce, Turkey | 51.52 | 89.26 | 99.01 |
| Hector Mine | 38.71 | 91.13 | 94.77 |
| Imperial Valley | 63.11 | 86.89 | 94.66 |
| Imperial Valley | 47.15 | 83.74 | 94.27 |
| Kobe, Japan | 54.14 | 82.71 | 97.42 |
| Kobe, Japan | 43.59 | 87.82 | 98.72 |
| Kocaeli, Turkey | 41.13 | 79.84 | 88.71 |
| Kocaeli, Turkey | 42.55 | 72.34 | 74.47 |
| Landers | 47.03 | 89.73 | 92.43 |
| Landers | 4.23 | 63.38 | 83.10 |
| Loma Prieta | 70.51 | 83.87 | 99.19 |
| Loma Prieta | 63.64 | 84.09 | 97.99 |
| Manjil, Iran | 39.88 | 89.88 | 95.78 |
| Superstition Hills | 30.77 | 86.54 | 93.99 |
| Superstition Hills | 59.88 | 88.95 | 98.77 |
| Cape Mendocino | 5.94 | 73.27 | 95.36 |
| Chi-Chi, Taiwan | 45.92 | 84.12 | 90.56 |
| Chi-Chi, Taiwan | 54.17 | 81.55 | 96.35 |
| San Fernando | 41.33 | 87.78 | 96.73 |
| Friuli, Italy | 48.98 | 71.43 | 97.63 |
| **Mean** | 46.02 | 83.51 | 94.44 |
| **Standard Deviation** | 16.4297 | 7.3814 | 5.9500 |
| **Maximum** | 70.51 | 92.33 | 99.19 |
| **Minimum** | 4.23 | 63.38 | 74.47 |

It can be observed from the Table 3 and Figure 10 that the response reduction capacity of the inertial amplifier coupled base isolator is better than CBI and Inerter-BI. The pattern of the displacement histogram plot is indicating as random distribution as it has several different peaks. The majority of the displacement reduction percentage for the IABI system wait between 80% to 100% while for the CBI

system, the majority shows from 1% to 70%, and for Inerter-BI, from 70% to 80%. The time history plots of the base shear are evaluated and presented in Figure 12(a-d) for similar earthquakes. IABI system performs significantly better than the CBI and Inerter-BI in terms of base shear reduction.

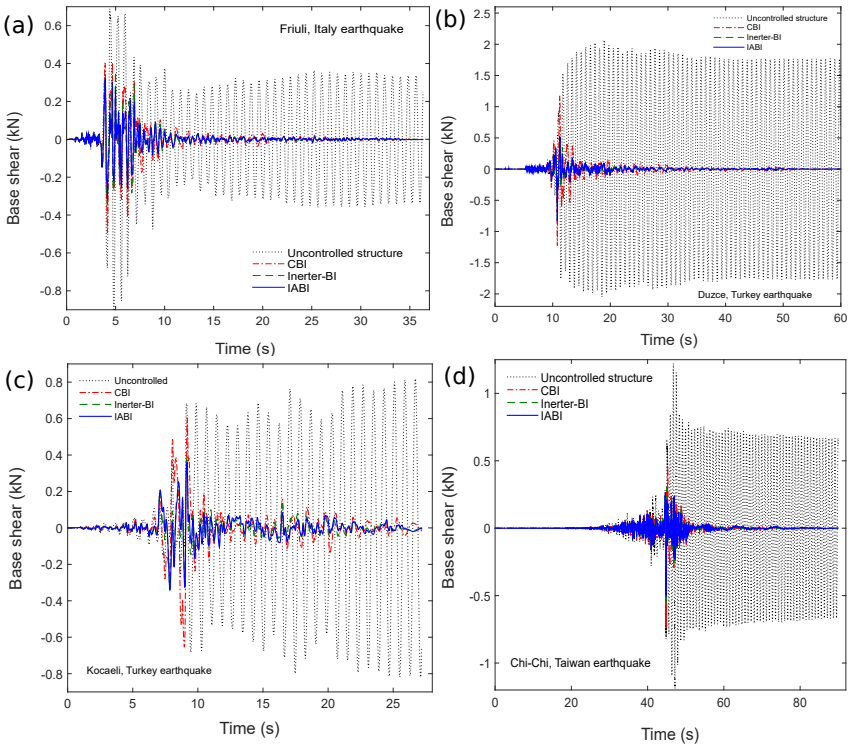


**Figure** 12: (a-d) Variations of the base shear of the structure with time for different earthquakes.

The histogram plot for the base shear reduction is indicating it as random distribution and shown in Figure 13. The majority of the reduction in base shear waits between 1% to 50% for CBI, 1% to 70% for Inerter-BI, while for inertial amplifier coupled base isolator it waits between 30% to 90%. Base shear reductions(%) for all adopted earthquakes are presented in Table 4.

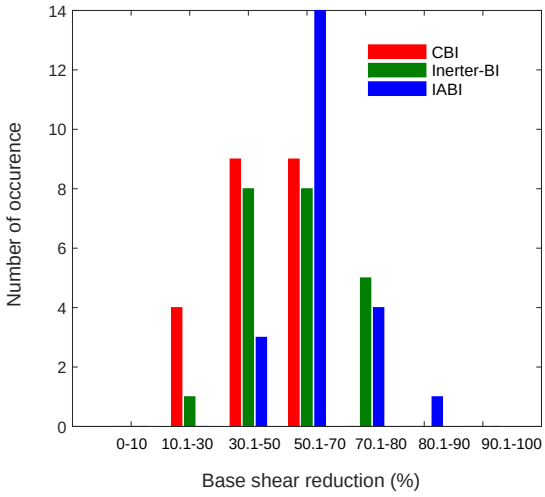


**Figure** 13: Variation of number of occurrence with range of reduction percentage of the base shear.

**Table** 4: Base shear reduction (%) of controlled structure with respect to uncontrolled structure for different earthquakes.

| **Earthquake** | **Base shear reduction(%)** | | |
|---|---|---|---|
| | **CBI** | **Inerter-BI** | **IABI** |
| Northridge | 57.07 | 76.13 | 78.73 |
| Northridge | 31.47 | 46.67 | 53.35 |
| Duzce, Turkey | 40.72 | 59.12 | 59.86 |
| Hector Mine | 56.93 | 71.01 | 72.50 |
| Imperial Valley | 63.31 | 72.95 | 74.37 |
| Imperial Valley | 36.51 | 61.18 | 63.09 |
| Kobe, Japan | 53.98 | 55.34 | 55.72 |
| Kobe, Japan | 54.12 | 74.54 | 74.97 |
| Kocaeli, Turkey | 40.19 | 63.08 | 64.38 |
| Kocaeli, Turkey | 30.88 | 45.92 | 47.29 |
| Landers | 63.68 | 77.13 | 82.44 |
| Landers | 16.70 | 38.18 | 43.40 |
| Loma Prieta | 54.15 | 63.96 | 66.40 |
| Loma Prieta | 12.82 | 29.92 | 37.97 |
| Manjil, Iran | 42.45 | 58.29 | 60.33 |
| Superstition Hills | 17.90 | 61.87 | 63.12 |
| Superstition Hills | 45.99 | 61.03 | 62.65 |
| Cape Mendocino | 36.09 | 46.05 | 56.94 |
| Chi-Chi, Taiwan | 54.19 | 66.90 | 68.86 |
| Chi-Chi, Taiwan | 38.74 | 56.58 | 58.95 |
| San Fernando | 25.75 | 49.26 | 53.06 |
| Friuli, Italy | 46.56 | 59.87 | 65.76 |
| **Mean** | 41.83 | 58.86 | 62.01 |
| **Standard Deviation** | 14.8780 | 12.3602 | 11.1150 |
| **Maximum** | 63.68 | 77.13 | 82.44 |
| **Minimum** | 12.82 | 29.92 | 37.97 |

The variations of kinetic energy, damping energy, and potential energy of structure and isolators are presented in Figure 14, Figure 15, and Figure 16.

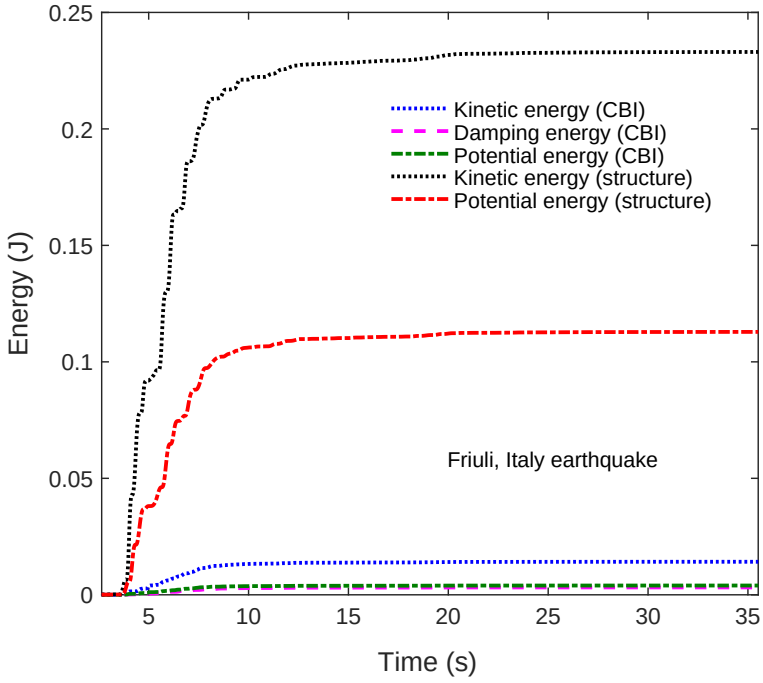


**Figure** 14: (a) Energy plots of the structure isolated by classical base isolation system under Friuli, Italy earthquake.

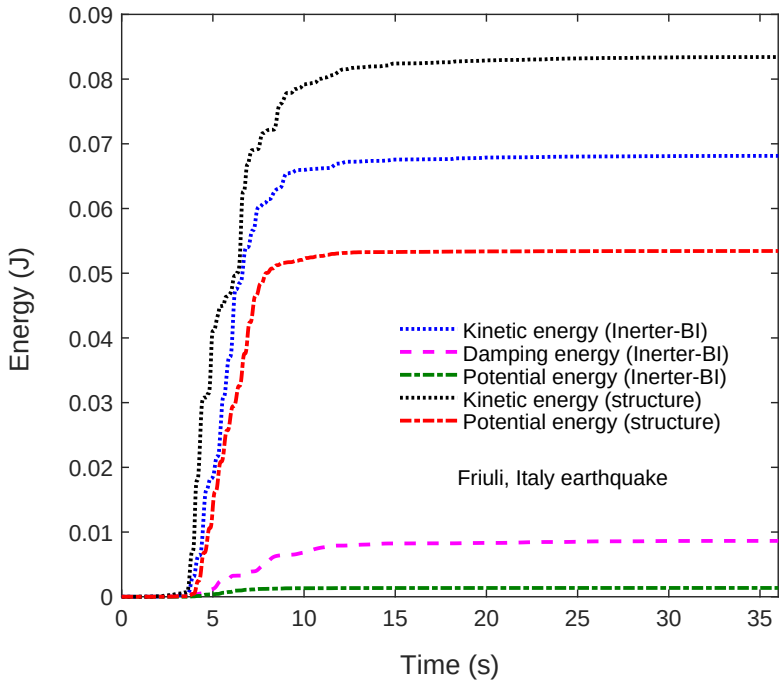


**Figure** 15: (a) Energy plots of the structure isolated by inerter-based isolation system under Friuli, Italy earthquake.

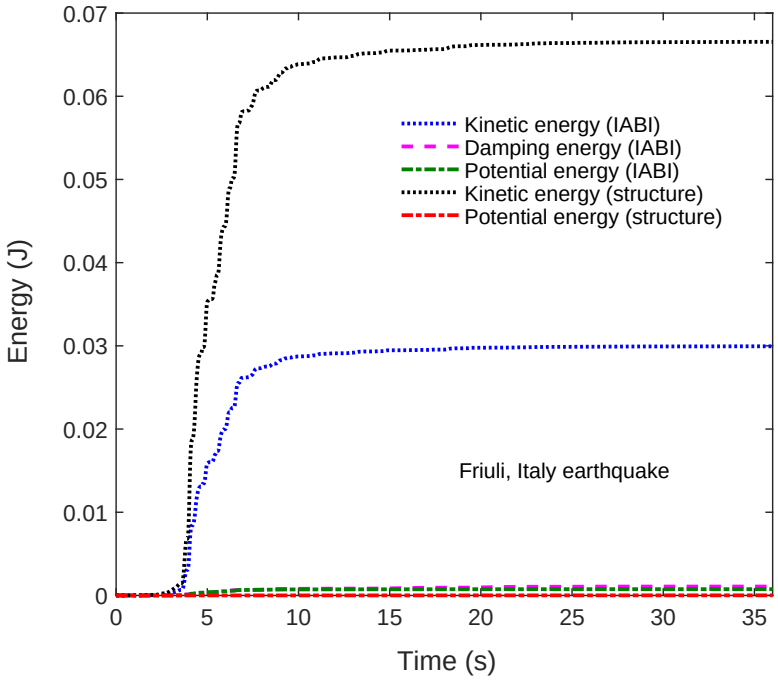


**Figure** 16: (a) Energy plots of the structure isolated by inertial amplifier coupled base isolator under Friuli, Italy earthquake.

The plots are proven the superior seismic performance of the proposed inertial amplifier coupled base isolator. The presented figures are evaluated due to the effect of Friuli, Italy earthquake ground motions. It is also seen that the nature of the energy plots for other earthquakes are similar.

## 6. Conclusions

A vibration base isolation system coupled with inertial amplifier has been proposed in the paper. An analytical solution has been developed to obtain the structural displacement of the amplified isolated system under harmonic ground motion. The frequency-domain results are also validated by the time history analysis. Standard deviation of the system response due to broadband random excitation has been obtained in closed-form. Twenty-two real earthquakes ground motions are implemented in the design to generate the earthquake responses. It can be concluded from the overall study that the seismic performance of the inertial amplifier coupled base isolator is significantly greater than the classical base isolation system. The proposed research can also be implemented in a practical scenario in the future. A fair comparison has been conducted between the inerter-based isolation system and inertial amplifier coupled base isolator to investigate the seismic performance and response reduction capacity, respectively. The key points of the proposed research are following:

- The underlying mechanics of the inertial amplifier coupled base isolator, introduced in this paper, is conceptually different from the well known flywheel-gear inerter [73] based base isolator.
- From the frequency domain results, it is observed that the seismic performance of proposed IABI system is 71.47% and 63.60% superior to the CBI and Inerter-BI. As all the systems are linear, the stochastic behaviour of the responses are similar to the responses evaluated under harmonic ground motions.
- It is also evidenced from the parametric study that with the help of smaller mass ratios of the inertial amplifier coupled base isolator to structure, the inertial angle between the stiffness spring and rigid link, and lower isolation damping, the proposed inertial isolation system mitigate the seismic responses most.
- It is also observed from the parametric study that for damping ratios less than 20% the peak displacement amplitude decreases, and it becomes pretty stable and approximately constant for higher damping values. The values of peak displacement amplitude of structure isolated by IABI are evaluated as 1.76, 1.44, 1.33, 1.34, 1.35, 1.36 for $0.05 < \zeta_{ib} < 0.50$.
- It is observed from the standard deviation solutions for structural displacement, acceleration and shear force of the structure that the favourable condition for the structural control achieved while the values of the effective mass of the inertial amplifier coupled base isolator ($m_{ia}$) and damping coefficient ($\zeta_{ib}$) increases.
- From the numerical study, it is observed that the response reduction capacity of the IABI is 89.38% and 72% superior to the CBI and Inerter-BI.

The results implied that the proposed inertial amplifier coupled base isolator can be successfully implemented in vibration control of various structures. Future study will be conducted towards it experimentation and implementation in bridges and multi-storied buildings to mitigated the vibration responses.

**Declaration of competing interest**

The authors declare that they have no known competing financial interests or personal relationships that could have appeared to influence the work reported in this paper

**Acknowledgement**

The authors' would like to acknowledge the Inspire faculty grant, grant number DST/ INSPIRE/04/2018/000052 for partial financial support for the project.

[1] J. Touaillon, Improvement in buildings, U.S. Patent No. 99,973 (Feb. 15 1870).
[2] E. Kazeminezhad, M. T. Kazemi, S. M. Mirhosseini, Assessment of the vertical stiffness of elastomeric bearing due to displacement and rotation, International Journal of Non-Linear Mechanics 119 (2020) 103306.
[3] J. Hwang, J. Chiou, An equivalent linear model of lead-rubber seismic isolation bearings, Engineering Structures 18 (7) (1996) 528–536.
[4] J. M. Kelly, Base isolation: linear theory and design, Earthquake spectra 6 (2) (1990) 223–244.
[5] N. Makris, Seismic isolation: Early history, Earthquake Engineering & Structural Dynamics 48 (2) (2019) 269–283.
[6] A. De Luca, L. G. Guidi, State of art in the worldwide evolution of base isolation design, Soil Dynamics and Earthquake Engineering 125 (2019) 105722.
[7] J. A. Inaudi, J. M. Kelly, Optimum damping in linear isolation systems, Earthquake engineering & structural dynamics 22 (7) (1993) 583–598.

[8] S. Adhikari, Qualitative dynamic characteristics of a non-viscously damped oscillator, Proceedings of the Royal Society of London, Series- A 461 (2059) (2005) 2269–2288.
[9] S. Adhikari, B. Pascual, Eigenvalues of linear viscoelastic systems, Journal of Sound and Vibration 325 (4-5) (2009) 1000–1011.
[10] A. Batou, S. Adhikari, Optimal parameters of viscoelastic tuned-mass dampers, Journal of Sound and Vibration 445 (4) (2019) 17–28.
[11] D. M. Lee, Base isolation for torsion reduction in asymmetric structures under earthquake loading, Earthquake Engineering & Structural Dynamics 8 (4) (1980) 349–359.
[12] M. C. Constantinou, I. G. Tadjbakhsh, Hysteretic dampers in base isolation: random approach, Journal of Structural Engineering 111 (4) (1985) 705–721.
[13] M. Eisenberger, A. Rutenberg, Seismic base isolation of asymmetric shear buildings, Engineering structures 8 (1) (1986) 2–8.
[14] W. H. Robinson, Lead-rubber hysteretic bearings suitable for protecting structures during earthquakes, Earthquake engineering & structural dynamics 10 (4) (1982) 593–604.
[15] I. G. Buckle, New zealand seismic base isolation concepts and their application to nuclear engineering, Nuclear Engineering and Design 84 (3) (1985) 313–326.
[16] R. Jangid, Optimum friction pendulum system for near-fault motions, Engineering Structures 27 (3) (2005) 349–359.
[17] R. Jangid, Computational numerical models for seismic response of structures isolated by sliding systems, Structural Control and Health Monitoring 12 (1) (2005) 117–137.
[18] H. Shakib, A. Fuladgar, Response of pure-friction sliding structures to three components of earthquake excitation, Computers & Structures 81 (4) (2003) 189–196.
[19] P. Castaldo, B. Palazzo, T. Ferrentino, Seismic reliability-based ductility demand evaluation for inelastic base-isolated structures with friction pendulum devices, Earthquake Engineering & Structural Dynamics 46 (8) (2017) 1245–1266.
[20] P. Castaldo, B. Palazzo, G. Alfano, M. F. Palumbo, Seismic reliability-based ductility demand for hardening and softening structures isolated by friction pendulum bearings, Structural Control and Health Monitoring 25 (11) (2018) e2256.
[21] A. Pavese, M. Furinghetti, C. Casarotti, Investigation of the consequences of mounting laying defects for curved surface slider devices under general seismic input, Journal of Earthquake Engineering 23 (3) (2019) 377–403.
[22] M. Furinghetti, I. Lanese, A. Pavese, Experimental assessment of the seismic response of a base-isolated building through a hybrid simulation, Recent Advances and Applications of Seismic Isolation and Energy Dissipation Devices.
[23] M. Furinghetti, T. Yang, P. M. Calvi, A. Pavese, Experimental evaluation of extra-stroke displacement capacity for curved surface slider devices, Soil Dynamics and Earthquake Engineering 146 (2021) 106752.
[24] S. Eliseev, Structural theory of vibration protection systems (1978).
[25] E. I. Rivin, Passive vibration isolation, 2003.
[26] M. C. Smith, Synthesis of mechanical networks: the inerter, IEEE Transactions on automatic control 47 (10) (2002) 1648–1662.
[27] M. C. Smith, The inerter: A retrospective, Annual Review of Control, Robotics, and Autonomous Systems 3 (2020) 361–391.
[28] M. C. Smith, F.-C. Wang, Performance benefits in passive vehicle suspensions employing inerters, Vehicle system dynamics 42 (4) (2004) 235–257.
[29] F.-C. Wang, M.-K. Liao, B.-H. Liao, W.-J. Su, H.-A. Chan, The performance improvements of train suspension systems with mechanical networks employing inerters, Vehicle System Dynamics 47 (7) (2009) 805–830.
[30] F.-C. Wang, C.-H. Yu, M.-L. Chang, M. Hsu, The performance improvements of train suspension systems with inerters, in: Proceedings of the 45th IEEE Conference on Decision and Control, IEEE, 2006, pp. 1472–1477.
[31] F.-C. Wang, M.-R. Hsieh, H.-J. Chen, Stability and performance analysis of a full-train system with inerters, Vehicle System Dynamics 50 (4) (2012) 545–571.
[32] Y. Hu, M. Z. Chen, Y. Sun, Comfort-oriented vehicle suspension design with skyhook inerter configuration, Journal of Sound and Vibration 405 (2017) 34–47.
[33] M. Z. Chen, Y. Hu, Inerter and Its Application in Vibration Control Systems, Springer, 2019.
[34] W. M. Kuhnert, P. J. P. Gonçalves, D. F. Ledezma-Ramirez, M. J. Brennan, Inerter-like devices used for vibration isolation: A historical perspective, Journal of the Franklin Institute.
[35] F. Qian, Y. Luo Sr, H. Sun, W. C. Tai, L. Zuo, Performance enhancement of a base-isolation structure using optimal tuned inerter dampers, in: Active and Passive Smart Structures and Integrated Systems XIII, Vol. 10967, International Society for Optics and Photonics, 2019, p. 1096715.
[36] H. Sun, L. Zuo, X. Wang, J. Peng, W. Wang, Exact h2 optimal solutions to inerter-based isolation systems for building structures, Structural Control and Health Monitoring 26 (6) (2019) e2357.
[37] Z. Zhao, Q. Chen, R. Zhang, C. Pan, Y. Jiang, Energy dissipation mechanism of inerter systems, International Journal of Mechanical Sciences 184 (2020) 105845.
[38] G. Moghimi, N. Makris, Seismic response of yielding structures equipped with inerters, Soil Dynamics and Earthquake Engineering (2020) 106474.
[39] L. Li, Q. Liang, Effect of inerter for seismic mitigation comparing with base isolation, Structural Control and Health Monitoring 26 (10) (2019) e2409.
[40] Y. Jiang, Z. Zhao, R. Zhang, D. De Domenico, C. Pan, Optimal design based on analytical solution for storage tank with inerter isolation system, Soil Dynamics and Earthquake Engineering 129 (2020) 105924.
[41] Z. Zhao, R. Zhang, N. E. Wierschem, Y. Jiang, C. Pan, Displacement mitigation–oriented design and mechanism for inerter-based isolation system, Journal of Vibration and Control (2020) 1077546320951662.
[42] D. De Domenico, G. Ricciardi, R. Zhang, Optimal design and seismic performance of tuned fluid inerter applied to structures with friction pendulum isolators, Soil Dynamics and Earthquake Engineering 132 (2020) 106099.
[43] Z. Zhao, R. Zhang, Y. Jiang, C. Pan, Seismic response mitigation of structures with a friction pendulum inerter system, Engineering Structures 193 (2019) 110–120.

[44] Z. Zhao, Q. Chen, R. Zhang, C. Pan, Y. Jiang, Optimal design of an inerter isolation system considering the soil condition, Engineering Structures 196 (2019) 109324.
[45] R. Zhang, Z. Zhao, C. Pan, Influence of mechanical layout of inerter systems on seismic mitigation of storage tanks, Soil Dynamics and Earthquake Engineering 114 (2018) 639–649.
[46] R. Zhang, Z. Zhao, K. Dai, Seismic response mitigation of a wind turbine tower using a tuned parallel inerter mass system, Engineering Structures 180 (2019) 29–39.
[47] A. A. Taflanidis, A. Giaralis, D. Patsialis, Multi-objective optimal design of inerter-based vibration absorbers for earthquake protection of multi-storey building structures, Journal of the Franklin Institute 356 (14) (2019) 7754–7784.
[48] D. Čakmak, Z. Tomičević, H. Wolf, Ž. Božić, D. Semenski, I. Trapić, Vibration fatigue study of the helical spring in the base-excited inerter-based isolation system, Engineering Failure Analysis 103 (2019) 44–56.
[49] M. Z. Chen, Y. Hu, Analysis for inerter-based vibration system, in: Inerter and Its Application in Vibration Control Systems, Springer, 2019, pp. 19–39.
[50] C. Yilmaz, G. M. Hulbert, N. Kikuchi, Phononic band gaps induced by inertial amplification in periodic media, Physical Review B 76 (5) (2007) 054309.
[51] S. Taniker, C. Yilmaz, Design, analysis and experimental investigation of three-dimensional structures with inertial amplification induced vibration stop bands, International Journal of Solids and Structures 72 (2015) 88–97.
[52] C. Yilmaz, G. Hulbert, Theory of phononic gaps induced by inertial amplification in finite structures, Physics Letters A 374 (34) (2010) 3576–3584.
[53] S. Taniker, C. Yilmaz, Phononic gaps induced by inertial amplification in bcc and fcc lattices, Physics Letters A 377 (31-33) (2013) 1930–1936.
[54] O. Yuksel, C. Yilmaz, Shape optimization of phononic band gap structures incorporating inertial amplification mechanisms, Journal of Sound and Vibration 355 (2015) 232–245.
[55] S. Taniker, C. Yilmaz, Generating ultra wide vibration stop bands by a novel inertial amplification mechanism topology with flexure hinges, International Journal of Solids and Structures 106 (2017) 129–138.
[56] O. Yuksel, C. Yilmaz, Realization of an ultrawide stop band in a 2-d elastic metamaterial with topologically optimized inertial amplification mechanisms, International Journal of Solids and Structures 203 (2020) 138–150.
[57] M. Barys, R. Zalewski, Analysis of inertial amplification mechanism with smart spring-damper for attenuation of beam vibrations, in: MATEC Web of Conferences, Vol. 157, EDP Sciences, 2018, p. 03002.
[58] C. Yilmaz, G. M. Hulbert, Dynamics of locally resonant and inertially amplified lattice materials, Dynamics of Lattice Materials; Phani, AS, Hussein, MI, Eds (2017) 233.
[59] Y. Mi, X. Yu, Sound transmission of acoustic metamaterial beams with periodic inertial amplification mechanisms, Journal of Sound and Vibration 499 (2021) 116009.
[60] J. Zhou, L. Dou, K. Wang, D. Xu, H. Ouyang, A nonlinear resonator with inertial amplification for very low-frequency flexural wave attenuations in beams, Nonlinear Dynamics 96 (1) (2019) 647–665.
[61] M. Barys, J. S. Jensen, N. M. Frandsen, Efficient attenuation of beam vibrations by inertial amplification, European Journal of Mechanics-A/Solids 71 (2018) 245–257.
[62] S. Muhammad, S. Wang, F. Li, C. Zhang, Bandgap enhancement of periodic nonuniform metamaterial beams with inertial amplification mechanisms, Journal of Vibration and Control (2020) 1077546319895630.
[63] F. Sun, X. Dai, Y. Liu, L. Xiao, Seismic mitigation performance of periodic foundations with inertial amplification mechanism considering superstructure-foundation interaction, Smart Materials and Structures 30 (2) (2021) 025018.
[64] N. M. Frandsen, O. R. Bilal, J. S. Jensen, M. I. Hussein, Inertial amplification of continuous structures: Large band gaps from small masses, Journal of Applied Physics 119 (12) (2016) 124902.
[65] Z. Cheng, A. Palermo, Z. Shi, A. Marzani, Enhanced tuned mass damper using an inertial amplification mechanism, Journal of Sound and Vibration (2020) 115267.
[66] M. Hou, J. H. Wu, S. Cao, D. Guan, Y. Zhu, Extremely low frequency band gaps of beam-like inertial amplification metamaterials, Modern Physics Letters B 31 (27) (2017) 1750251.
[67] G. Yilmaz, Hulbert, and n. kikuchi,phononic band gaps induced by inertial amplification in periodic media,, Phys. Rev. B 76 (2007) 054309.
[68] M. Miniaci, M. Mazzotti, A. Amendola, F. Fraternali, Inducing dispersion curves with negative group velocity in inertially amplified phononic crystals through the application of an external state of prestress, in: XI International Conference on Structural Dynamic, EURODYN 2020, 2020, pp. 612–620.
[69] J. B. Roberts, P. D. Spanos, Random vibration and statistical linearization, Courier Corporation, 2003.
[70] S. Adhikari, B. Pascual, The 'damping effect' in the dynamic response of stochastic oscillators, Probabilistic Engineering Mechanics 44 (4) (2016) 2–17.
[71] E. Jacquelin, D. Brizard, S. Adhikari, M. I. Friswel, Time-domain response of damped stochastic multiple-degree-of-freedom systems, ASCE Journal of Engineering Mechanics 146 (1) (2020) 06019005:1–7.
[72] A. Banerjee, A. Chanda, R. Das, Seismic analysis of a curved bridge considering deck-abutment pounding interaction: an analytical investigation on the post-impact response, Earthquake Engineering & Structural Dynamics 46 (2) (2017) 267–290.
[73] A. Kras, P. Gardonio, Active vibration control unit with a flywheel inertial actuator, Journal of Sound and Vibration 464 (2020) 114987.